

Development of an eight-band theory for quantum-dot heterostructures

E. P. Pokatilov[†] and V. A. Fonoberov[‡]

*Laboratory of Multilayer Structure Physics, Department of Theoretical Physics,
State University of Moldova, A. Mateevici 60, MD-2009 Chişinău, Moldova*

V. M. Fomin[§] and J. T. Devreese^{*}

*Theoretische Fysica van de Vaste Stof, Departement Natuurkunde,
Universiteit Antwerpen (UIA), Universiteitsplein 1, B-2610 Antwerpen, België*
(October 26, 2018)

Abstract

We derive a nonsymmetrized 8-band effective-mass Hamiltonian for quantum-dot heterostructures (QDHs) in Burt's envelope-function representation. The 8×8 radial Hamiltonian and the boundary conditions for the Schrödinger equation are obtained for spherical QDHs. Boundary conditions for symmetrized and nonsymmetrized radial Hamiltonians are compared with each other and with connection rules that are commonly used to match the wave functions found from the bulk $\mathbf{k} \cdot \mathbf{p}$ Hamiltonians of two adjacent materials. Electron and hole energy spectra in three spherical QDHs: HgS/CdS, InAs/GaAs, and GaAs/AlAs are calculated as a function of the quantum dot radius within the approximate symmetrized and exact nonsymmetrized 8×8 models. The parameters of dissymmetry are shown to influence the energy levels and the wave functions of an electron and a hole and, consequently, the energies of both intraband and interband transitions.

PACS numbers: 73.20.Dx, 73.40.Kp, 73.40.Lq

I. INTRODUCTION

The 4×4 $\mathbf{k} \cdot \mathbf{p}$ hole Hamiltonian for the wave function envelopes (so called effective-mass Hamiltonian), that takes into account mixing of the light- and heavy-hole bands, was obtained in Ref. 1 using the perturbation theory. This multiband Hamiltonian has been employed for description of the hole states in bulk crystals² as well as in low-dimensional structures, in particular, in free-standing homogeneous quantum dots (QDs)^{3,4}. The inclusion of the mixing with the spin-orbit split-off hole band leads to the 6×6 $\mathbf{k} \cdot \mathbf{p}$ Hamiltonian which has also been applied^{5,6} to QDs. To consider the nonparabolicity of the electron dispersion in narrow- and medium-gap semiconductors, it is necessary to take into account the coupling of the conduction and valence bands. Using the $\mathbf{k} \cdot \mathbf{p}$ perturbation theory for bulk semiconductors with cubic lattice symmetry, the 8×8 $\mathbf{k} \cdot \mathbf{p}$ model was developed in Ref. 7.

This model explicitly includes eight bands around the Γ point of the Brillouin zone, namely, electron, heavy-, light-, and spin-orbit split-off hole bands (each of them is twice-degenerate due to the spin), and treats all other bands as remote. Along with more simple models, the 8×8 $\mathbf{k} \cdot \mathbf{p}$ Hamiltonian has been used to investigate different QDs (see, e. g. Refs. 8–11).

Recently, one has begun to apply multiband effective-mass Hamiltonians to investigate elastic, electronic, and optical properties of multilayer nanostructures such as quantum-dot heterostructures (QDHs): CdS/HgS¹¹, InAs/GaAs^{12,13}, GaAs/Al_xGa_{1-x}As^{14,15}, and CdS/HgS/CdS/H₂O^{16,17}. However, it should be emphasized, that multiband $\mathbf{k} \cdot \mathbf{p}$ Hamiltonians are derived for homogeneous bulk materials, i.e. under the assumption that all effective-mass parameters are *constant*. This is important, because at a certain step of the derivation, wavenumbers \mathbf{k} are declared as operators $\hat{\mathbf{p}}/\hbar$ that do not commute with the functions of coordinates. But, at the heterointerfaces of the multilayer nanostructures, there occurs an abrupt change of effective-mass parameters from their values in one material to those in the adjacent material. Inside a thin transitional layer that contains the heterointerface, the ordering of the differential operators and coordinate-dependent effective-mass parameters in the multiband Hamiltonian becomes crucial. In QDs with an infinitely high confining potential for electrons and holes, all components of the wave function vanish at the heterointerface, and there remains a possibility of applying the bulk multiband $\mathbf{k} \cdot \mathbf{p}$ Hamiltonian straightforwardly.^{3–6,8–11} There are two ways to proceed from QDs to QDHs.

(i) The first way is to use an appropriate bulk multiband Hamiltonian for each constituent material separately, and then to match the obtained homogeneous solutions at the abrupt heterojunctions applying the *connection rules* (CRs) that are usually obtained by imposing the continuity of the wave function envelopes and of the normal to the heterointerface component of the velocity.^{11,16} It should be underlined that this way is heuristic and nonunique. In Ref. 18 the general CRs, that even do not require the continuity of the wave function envelopes, have been proposed for planar heterostructures.

(ii) The second way (cf. Refs. 19–21) is to derive a multiband Hamiltonian valid for the entire heterostructure, including the heterointerfaces, and then, if material parameters change abruptly at some interfaces, to find the *boundary conditions* (BCs) for the solutions of the envelope function equation. To find these BCs, one should use the multiband envelope function equation $(\hat{H} - E)\Psi = 0$ at any point of the heterostructure, including the heterointerfaces, and integrate this equation over the volume of an infinitely thin layer, which includes the considered heterointerface. Thus, the BCs are derived starting from the requirement of continuity of the components of the wave function at the heterointerface.

One can always choose the CRs physically equivalent to the BCs.²² The both approaches (i) and (ii) are usually used when the wave function inside each layer of a heterostructure can be found analytically, for example in planar or spherical heterostructures. In case of an arbitrary shape of the heterointerface, the approach (ii) can still be used because, when the Hamiltonian is known for the entire heterostructure, one can find an overall numerical solution of the Schrödinger equation.

A commonly used heuristic method to obtain a multiband effective-mass Hamiltonian for heterostructures uses symmetrization^{23–27} of the corresponding $\mathbf{k} \cdot \mathbf{p}$ Hamiltonian. This method consists in the symmetrical arrangement of the components of the momentum operator, that ensures the hermicity of the resulting Hamiltonian. Namely $\beta \hat{\mathbf{p}} \rightarrow (\beta(\mathbf{r}) \hat{\mathbf{p}} + \hat{\mathbf{p}} \beta(\mathbf{r})) / 2$ and $\beta \hat{p}_i \hat{p}_j \rightarrow (\hat{p}_i \beta(\mathbf{r}) \hat{p}_j + \hat{p}_j \beta(\mathbf{r}) \hat{p}_i) / 2$, where $\beta(\mathbf{r})$ is a spatially

varying effective-mass or other material-dependent parameter which is usually considered a piece-wise constant, because in each layer of a heterostructure it has the value for a corresponding bulk material. The symmetrization has been applied to QDHs in Refs. 12,13,17. An essential fault of the symmetrization is that it is not a *necessary* condition for the multiband Hamiltonian to be hermitian. Besides that, as will be seen below, some intrinsic properties of the heterointerface, such as reducing the symmetry of the problem and smoothing the abrupt change of the effective-mass parameters at a heterojunction, are completely neglected in the symmetrized Hamiltonian.

Burt has derived^{19–21} the exact envelope-function equations for a heterostructure. The order of the components of the momentum operator arises as a part of that derivation. This theory has been used by Foreman to explicitly write the 6×6 (Ref. 28) and 8×8 (Ref. 29) effective-mass Hamiltonians for planar heterostructures. General rules for constructing the valence-band effective-mass Hamiltonians with a correct operator ordering have been described in Ref. 30 for the heterostructures with arbitrary crystallographic orientations. In Ref. 31,32, correct boundary conditions for planar heterostructures with wurtzite symmetry have been presented. Comparing the conduction- and valence-subband dispersion of a planar quantum well, calculated using the BCs following from the exact nonsymmetrized and from the symmetrized effective-mass Hamiltonians, it has been shown that the former BCs give physically reasonable results, while the latter BCs can produce nonphysical solutions.^{28,33} More recently, these two sets of BCs for a planar quantum well have been examined within the tight-binding approach.³⁴ The result of the comparison allowed to give preference to the nonsymmetrized model resulting from Burt’s derivation of the envelope-function Hamiltonian, which was shown to give reliable results even when the well and barrier effective-mass parameters were very dissimilar.

In the present paper the envelope-function representation of Refs. 19–21 is used to construct the nonsymmetrized 8-band Hamiltonian for an arbitrary 3-dimensional heterostructure. As an application, the electronic structure of two-layer HgS/CdS, InAs/GaAs, and GaAs/AlAs spherical QDHs is investigated as a function of the dot radius.

It should be mentioned that the *spurious solutions* (“oscillating”³⁵ states and “gap” states^{11,35}) did not become apparent in the aforementioned QDHs. However, such solutions may appear for a different set of parameters.

The results of the calculation are compared with those obtained from the symmetrized 8×8 Hamiltonian. The rest of the paper is organized as follows. In Sec. II the derivation of the nonsymmetrized 8-band Hamiltonian for a QDH is presented. The corresponding radial Hamiltonian for a spherical QDH is obtained in Sec. III. In Sec. IV the BCs for both symmetrized and nonsymmetrized radial Hamiltonians are compared with each other and with commonly used CRs. The results of the numerical calculation for spherical QDHs are obtained and discussed in Sec. V. Conclusions are given in Sec. VI. The 2×2 electron and 6×6 hole energy-dependent nonsymmetrized Hamiltonians for a QDH, as well as radial Hamiltonians and corresponding BCs for a spherical QDH are found in Appendix B from the nonsymmetrized 8-band Hamiltonians.

II. NONSYMMETRIZED 8-BAND HAMILTONIAN

We begin our derivation with the nonsymmetrized 8-band effective-mass Hamiltonian for a heterostructure, when the spin-orbit coupling is “turned-off”. In the Bloch function basis $|S\rangle, |X\rangle, |Y\rangle, |Z\rangle$ this Hamiltonian is represented in the following form²⁹

$$\hat{H}_4 = \frac{\hbar^2}{2m_0} \begin{pmatrix} \varepsilon_c + \hat{\mathbf{k}}\alpha\hat{\mathbf{k}} & \frac{i}{2}(v_1\hat{k}_x + \hat{k}_x v_2) & \frac{i}{2}(v_1\hat{k}_y + \hat{k}_y v_2) & \frac{i}{2}(v_1\hat{k}_z + \hat{k}_z v_2) \\ -\frac{i}{2}(v_2\hat{k}_x + \hat{k}_x v_1) & \varepsilon'_v - \hat{k}_x\beta_l\hat{k}_x - \hat{\mathbf{k}}_x^\perp\beta_h\hat{\mathbf{k}}_x^\perp & -3(\hat{k}_x\gamma_3^+\hat{k}_y + \hat{k}_y\gamma_3^-\hat{k}_x) & -3(\hat{k}_x\gamma_3^+\hat{k}_z + \hat{k}_z\gamma_3^-\hat{k}_x) \\ -\frac{i}{2}(v_2\hat{k}_y + \hat{k}_y v_1) & -3(\hat{k}_x\gamma_3^-\hat{k}_y + \hat{k}_y\gamma_3^+\hat{k}_x) & \varepsilon'_v - \hat{k}_y\beta_l\hat{k}_y - \hat{\mathbf{k}}_y^\perp\beta_h\hat{\mathbf{k}}_y^\perp & -3(\hat{k}_y\gamma_3^+\hat{k}_z + \hat{k}_z\gamma_3^-\hat{k}_y) \\ -\frac{i}{2}(v_2\hat{k}_z + \hat{k}_z v_1) & -3(\hat{k}_x\gamma_3^-\hat{k}_z + \hat{k}_z\gamma_3^+\hat{k}_x) & -3(\hat{k}_y\gamma_3^-\hat{k}_z + \hat{k}_z\gamma_3^+\hat{k}_y) & \varepsilon'_v - \hat{k}_z\beta_l\hat{k}_z - \hat{\mathbf{k}}_z^\perp\beta_h\hat{\mathbf{k}}_z^\perp \end{pmatrix}, \quad (1)$$

where $\varepsilon'_v = \varepsilon_v - \delta/3$, $\hat{\mathbf{k}} = -i\nabla$, $\hat{\mathbf{k}}_{x,y,z}^\perp = \hat{\mathbf{k}} - \hat{\mathbf{k}}_{x,y,z}$, $\beta_l = \gamma_1 + 4\gamma_2$, $\beta_h = \gamma_1 - 2\gamma_2$,

$$v_1 = v + \xi, \quad v_2 = v - \xi, \quad (2)$$

$$\gamma_3^+ = \gamma_3 + \chi, \quad \gamma_3^- = \gamma_3 - \chi. \quad (3)$$

ξ and χ are called the dissymmetry parameters, because when $\xi = 0$ and $\chi = 0$, the Hamiltonian (1) becomes symmetrical. The explicit form of the parameter $\xi \equiv (v_1 - v_2)/2$ follows from the formulae (A1) and (A2) in Appendix A, and the parameter χ is determined by Eq. (7).

When the spin-orbit coupling is “turned-on”, the considered 8-band Hamiltonian is represented in the Bloch function basis $|S\uparrow\rangle, |X\uparrow\rangle, |Y\uparrow\rangle, |Z\uparrow\rangle, |S\downarrow\rangle, |X\downarrow\rangle, |Y\downarrow\rangle, |Z\downarrow\rangle$ as

$$\hat{H}_8 = \begin{pmatrix} \hat{H}_4 & 0 \\ 0 & \hat{H}_4 \end{pmatrix} + H_{so}, \quad (4)$$

where \hat{H}_4 is defined by Eq. (1) and the spin-orbit Hamiltonian H_{so} has the form²⁵

$$H_{so} = \frac{\Delta}{3} \begin{pmatrix} 0 & 0 & 0 & 0 & 0 & 0 & 0 & 0 \\ 0 & 0 & -i & 0 & 0 & 0 & 0 & 1 \\ 0 & i & 0 & 0 & 0 & 0 & 0 & -i \\ 0 & 0 & 0 & 0 & 0 & -1 & i & 0 \\ 0 & 0 & 0 & 0 & 0 & 0 & 0 & 0 \\ 0 & 0 & 0 & -1 & 0 & 0 & i & 0 \\ 0 & 0 & 0 & -i & 0 & -i & 0 & 0 \\ 0 & 1 & i & 0 & 0 & 0 & 0 & 0 \end{pmatrix}. \quad (5)$$

In Eq. (1), m_0 is the free-electron mass, $E_c = \hbar^2\varepsilon_c/2m_0$ is the energy of the conduction band (CB) minimum, $E_v = \hbar^2\varepsilon_v/2m_0$ is the energy of the valence band (VB) maximum, $\Delta = \hbar^2\delta/2m_0$ is the spin-orbit splitting of the VB, and $V = \hbar v/2m_0$ is the Kane velocity ($V = -i\hbar\langle S|\hat{k}_z|Z\rangle/m_0$). Contributions of remote bands to the hole effective masses are written in terms of the “modified” Luttinger parameters $\gamma_1 = \gamma_1^L - E_p/3E_g$, $\gamma_2 = \gamma_2^L - E_p/6E_g$, and $\gamma_3 = \gamma_3^L - E_p/6E_g$, where $E_g = E_c - E_v$ is the energy gap, $E_p = 2m_0V^2$ is the

Kane energy, and γ_i^L ($i = 1, 2, 3$) are the Luttinger parameters of the VB. Parameter α can be evaluated through the experimentally determined CB-mass m_c using the relation

$$\frac{1}{m_c} = \frac{1}{m_0} \left(\alpha + \frac{E_p}{3} \left[\frac{2}{E_g} + \frac{1}{E_g + \Delta} \right] \right). \quad (6)$$

It is worth noting that all parameters entering the Hamiltonian (4) are coordinate-dependent. In a heterostructure these parameters abruptly change from their values in one material to the corresponding values in the adjacent material, therefore they are piecewise-constant functions of \mathbf{r} . Although not symmetrical, the Hamiltonian \hat{H}_8 is hermitian as seen from Eq. (4). The parameters ξ and χ (see Eqs. (2) and (3)) are responsible for the nonsymmetrical form of the Hamiltonian (4). The symmetrized 8-band Hamiltonian can be obtained, therefore, taking $\xi = 0$ and $\chi = 0$.

In Eq. (3), γ_3^+ is the contribution to γ_3 from the Γ_1 and Γ_{12} remote bands, while γ_3^- is the contribution to γ_3 from the Γ_{15} and Γ_{25} remote bands.²⁹ Neglecting small contributions from the Γ_{25} remote bands, the parameter $\chi(\mathbf{r})$ is determined as²⁹

$$\chi(\mathbf{r}) = (2\gamma_2(\mathbf{r}) + 3\gamma_3(\mathbf{r}) - \gamma_1(\mathbf{r}) - 1)/3, \quad (7)$$

i.e. it is explicitly defined by the effective-mass parameters of the bulk model. It is seen from Eq. (7) that in a homogeneous medium when $\gamma_i(\mathbf{r})$ are constants, $\chi(\mathbf{r})$ is also a constant, and therefore, it cancels from Eq. (1). Consequently, $\chi(\mathbf{r})$ is a specific function of a heterostructure, which gives a nonzero contribution to the Hamiltonian only at the heterointerfaces. The value of this contribution at the point \mathbf{r}_0 of a heterointerface is proportional to $\chi(\mathbf{r}_0 + \mathbf{e}_n) - \chi(\mathbf{r}_0 - \mathbf{e}_n)$, where \mathbf{e}_n is an infinitesimally small vector, normal to the heterointerface at the point \mathbf{r}_0 . Parameters $v_1(\mathbf{r})$ and $v_2(\mathbf{r})$ of the Hamiltonian (1), which can be obtained from the general effective mass equations as derived by Burt¹⁹, are given in Appendix A. In the definition (2), the functions $v_1(\mathbf{r})$ and $v_2(\mathbf{r})$ are subdivided into the symmetric $v(\mathbf{r})$ and antisymmetric $\xi(\mathbf{r})$ parts, where $\xi(\mathbf{r})$, like $\chi(\mathbf{r})$ above, is a specific parameter of a heterostructure. In general, $\xi(\mathbf{r})$ is a piecewise-constant function of \mathbf{r} . The necessary and sufficient condition for $\xi(\mathbf{r})$ to give a nonzero contribution to the 8×8 Hamiltonian only at the heterointerfaces, and to become a constant in the homogeneous medium, simultaneously with $v(\mathbf{r})$, is

$$\xi(\mathbf{r}) = c_\xi v(\mathbf{r}), \quad (8)$$

where the coefficient of proportionality c_ξ is constant over the entire heterostructure. Eq. (8) is the general form of $\xi(\mathbf{r})$ only for a two-layer heterostructure. For an N -layer heterostructure, there can be $N - 1$ independent constants – one for each heterointerface. Each constant for a given heterointerface can be found experimentally considering a two-layer heterostructure (see Sec. V).

In order to diagonalize the spin-orbit Hamiltonian H_{so} , it is convenient to carry out a unitary transformation of the Bloch function basis $|S\uparrow\rangle, |X\uparrow\rangle, |Y\uparrow\rangle, |Z\uparrow\rangle, |S\downarrow\rangle, |X\downarrow\rangle, |Y\downarrow\rangle, |Z\downarrow\rangle$ into the following Bloch function basis⁹

$$\begin{aligned} u_{1/2,1/2}^c &= |S\uparrow\rangle, \\ u_{1/2,-1/2}^c &= |S\downarrow\rangle, \end{aligned} \quad (9)$$

$$\begin{aligned}
u_{3/2,3/2}^v &= \frac{1}{\sqrt{2}}(|X\uparrow\rangle + i|Y\uparrow\rangle), \\
u_{3/2,1/2}^v &= \frac{i}{\sqrt{6}}(|X\downarrow\rangle + i|Y\downarrow\rangle - 2|Z\uparrow\rangle), \\
u_{3/2,-1/2}^v &= \frac{1}{\sqrt{6}}(|X\uparrow\rangle - i|Y\uparrow\rangle + 2|Z\downarrow\rangle), \\
u_{3/2,-3/2}^v &= \frac{i}{\sqrt{2}}(|X\downarrow\rangle - i|Y\downarrow\rangle), \\
u_{1/2,1/2}^v &= \frac{1}{\sqrt{3}}(|X\downarrow\rangle + i|Y\downarrow\rangle + |Z\uparrow\rangle), \\
u_{1/2,-1/2}^v &= \frac{-i}{\sqrt{3}}(|X\uparrow\rangle - i|Y\uparrow\rangle - |Z\downarrow\rangle),
\end{aligned} \tag{10}$$

where $u_{J,\mu}^c$ and $u_{J,\mu}^v$ are the Bloch functions of the conduction and valence bands, J is the Bloch function angular momentum, and $\mu \equiv J_z$ is its z -component. The 8-band Hamiltonian \hat{H} in the new basis can be obtained now after a unitary transformation

$$\hat{H} = U^* \hat{H}_8 U^T, \tag{11}$$

where U is the matrix of the transformation from the basis $\{|S\uparrow\rangle, |X\uparrow\rangle, |Y\uparrow\rangle, |Z\uparrow\rangle, |S\downarrow\rangle, |X\downarrow\rangle, |Y\downarrow\rangle, |Z\downarrow\rangle\}$ to the new basis $\{u_{1/2,1/2}^c, u_{1/2,-1/2}^c, u_{3/2,3/2}^v, u_{3/2,1/2}^v, u_{3/2,-1/2}^v, u_{3/2,-3/2}^v, u_{1/2,1/2}^v, u_{1/2,-1/2}^v\}$. U is defined by Eqs. (9) and (10). Performing the transformation (11), one obtains:

$$\hat{H} = \frac{\hbar^2}{2m_0} \begin{pmatrix} \varepsilon_c + T & 0 & iV_1 & \sqrt{\frac{2}{3}}V_0 & \frac{i}{\sqrt{3}}V_{-1} & 0 & \frac{i}{\sqrt{3}}V_0 & \sqrt{\frac{2}{3}}V_{-1} \\ 0 & \varepsilon_c + T & 0 & \frac{-1}{\sqrt{3}}V_1 & i\sqrt{\frac{2}{3}}V_0 & -V_{-1} & i\sqrt{\frac{2}{3}}V_1 & \frac{-1}{\sqrt{3}}V_0 \\ -iV_1^\dagger & 0 & \varepsilon_v - P - Q & -S & -R & 0 & \frac{-i}{\sqrt{2}}S & i\sqrt{2}R \\ \sqrt{\frac{2}{3}}V_0^\dagger & \frac{-1}{\sqrt{3}}V_1^\dagger & -S^\dagger & \varepsilon_v - P + Q & -C & -R & i\sqrt{2}Q & -i\sqrt{\frac{3}{2}}\Sigma \\ \frac{-i}{\sqrt{3}}V_{-1}^\dagger & -i\sqrt{\frac{2}{3}}V_0^\dagger & -R^\dagger & -C^\dagger & \varepsilon_v - P^* + Q^* & S^T & i\sqrt{\frac{3}{2}}\Sigma^* & i\sqrt{2}Q^* \\ 0 & -V_{-1}^\dagger & 0 & -R^\dagger & S^* & \varepsilon_v - P^* - Q^* & i\sqrt{2}R^\dagger & \frac{i}{\sqrt{2}}S^* \\ \frac{-i}{\sqrt{3}}V_0^\dagger & -i\sqrt{\frac{2}{3}}V_1^\dagger & \frac{i}{\sqrt{2}}S^\dagger & -i\sqrt{2}Q & -i\sqrt{\frac{3}{2}}\Sigma^T & -i\sqrt{2}R & \varepsilon_v'' - P & C \\ \sqrt{\frac{2}{3}}V_{-1}^\dagger & \frac{-1}{\sqrt{3}}V_0^\dagger & -i\sqrt{2}R^\dagger & i\sqrt{\frac{3}{2}}\Sigma^\dagger & -i\sqrt{2}Q^* & \frac{-i}{\sqrt{2}}S^T & C^\dagger & \varepsilon_v'' - P^* \end{pmatrix}, \tag{12}$$

where $\varepsilon_v'' = \varepsilon_v - \delta$,

$$\hat{k}_+ = \frac{\hat{k}_x + i\hat{k}_y}{\sqrt{2}}, \quad \hat{k}_- = \frac{\hat{k}_x - i\hat{k}_y}{\sqrt{2}},$$

$$\begin{aligned}
V_1 &= \frac{1}{2} (v_1 \hat{k}_+ + \hat{k}_+ v_2), & V_{-1} &= \frac{1}{2} (v_1 \hat{k}_- + \hat{k}_- v_2), \\
V_0 &= \frac{1}{2} (v_1 \hat{k}_z + \hat{k}_z v_2), & T &= \hat{k}_+ \alpha \hat{k}_- + \hat{k}_- \alpha \hat{k}_+ + \hat{k}_z \alpha \hat{k}_z, \\
P &= \hat{k}_+ (\gamma_1 - 2\chi) \hat{k}_- + \hat{k}_- (\gamma_1 + 2\chi) \hat{k}_+ + \hat{k}_z \gamma_1 \hat{k}_z, \\
Q &= \hat{k}_+ (\gamma_2 - \chi) \hat{k}_- + \hat{k}_- (\gamma_2 + \chi) \hat{k}_+ - 2\hat{k}_z \gamma_2 \hat{k}_z, \\
R &= \sqrt{3} (\hat{k}_+ (\gamma_2 - \gamma_3) \hat{k}_+ + \hat{k}_- (\gamma_2 + \gamma_3) \hat{k}_-), \\
S &= -i\sqrt{6} (\hat{k}_- (\gamma_3 + \chi) \hat{k}_z + \hat{k}_z (\gamma_3 - \chi) \hat{k}_-), \\
\Sigma &= -i\sqrt{6} \left(\hat{k}_- (\gamma_3 - \frac{\chi}{3}) \hat{k}_z + \hat{k}_z (\gamma_3 + \frac{\chi}{3}) \hat{k}_- \right), \\
C &= -i2\sqrt{2} (\hat{k}_- \chi \hat{k}_z - \hat{k}_z \chi \hat{k}_-). \tag{13}
\end{aligned}$$

In Eq. (12), daggers (\dagger) denote the hermitian conjugation, i.e. $A^\dagger \equiv (A^T)^*$ (it is important to note, that $(v_{1,2} \hat{k}_\pm)^\dagger = \hat{k}_\mp v_{1,2}$ and $(v_{1,2} \hat{k}_z)^\dagger = \hat{k}_z v_{1,2}$). Unlike the bulk 8×8 $\mathbf{k} \cdot \mathbf{p}$ Hamiltonian⁹ where the matrix element C is zero, in the Hamiltonian (12) the Bloch functions $u_{3/2,1/2}^v$ and $u_{3/2,-1/2}^v$ are coupled with each other, as well as the functions $u_{1/2,1/2}^v$ and $u_{1/2,-1/2}^v$. As seen from Eq. (13), this coupling arises because of the dissymmetry parameter χ , which can reduce, in this way, the symmetry of the problem. The Hamiltonian so obtained can be used to investigate electronic properties of quantum-well, quantum-wire, and quantum-dot heterostructures.

III. 8-BAND HAMILTONIAN FOR A SPHERICAL QDH

To study the electronic structure of spherical QDHs, the spherical approximation² (i.e. $\gamma_2^L = \gamma_3^L \equiv \gamma^L$) can be applied. If we take $\gamma^L = (2\gamma_2^L + 3\gamma_3^L)/5$, then the quantum states so obtained are correct to the first order of the perturbation theory. Using the relations between the Luttinger parameters γ_i^L and the ‘‘modified’’ Luttinger parameters γ_i we have

$$\gamma = (2\gamma_2 + 3\gamma_3)/5, \tag{14}$$

and according to Eq. (7)

$$\chi = (5\gamma - \gamma_1 - 1)/3. \tag{15}$$

In spherical QDHs, where all effective-mass parameters depend only on the absolute value r of the radius-vector, electron and hole states are eigenfunctions of the total angular momentum j and its z -component $m \equiv j_z$. Therefore, the electron or hole wave function can be written as a linear expansion in the eight Bloch functions $u_{J,\mu}^{c(v)}$:

$$\Psi_{j,m}(\mathbf{r}) = \sum_{J,\mu} F_{J,\mu}^{c;j,m}(\mathbf{r}) u_{J,\mu}^c + \sum_{J,\mu} F_{J,\mu}^{v;j,m}(\mathbf{r}) u_{J,\mu}^v, \tag{16}$$

where the envelope functions $F_{J,\mu}^{c(v);j,m}(\mathbf{r})$ are defined in the chosen Bloch function basis (9), (10) as

$$\begin{aligned} F_{1/2,\mu}^{c;j,m}(\mathbf{r}) &= \sum_{l,\lambda} C_{1/2,\mu;l,\lambda}^{j,m} R_{1/2,l}^{c;j}(r) Y_{l,\lambda}(\theta, \phi), \\ F_{3/2,\mu}^{v;j,m}(\mathbf{r}) &= i^{\mu-3/2} \sum_{l,\lambda} C_{3/2,\mu;l,\lambda}^{j,m} R_{3/2,l}^{v;j}(r) Y_{l,\lambda}(\theta, \phi), \\ F_{1/2,\mu}^{v;j,m}(\mathbf{r}) &= i^{1/2-\mu} \sum_{l,\lambda} C_{1/2,\mu;l,\lambda}^{j,m} R_{1/2,l}^{v;j}(r) Y_{l,\lambda}(\theta, \phi). \end{aligned} \quad (17)$$

Here, $R_{J,l}^{c(v);j}(r)$ are the radial envelope functions, $C_{J,\mu;l,\lambda}^{j,m}$ are the Clebsch-Gordan coefficients, and $Y_{l,\lambda}(\theta, \phi)$ are the spherical harmonics. Noting that in the matrix representation of the Hamiltonian (12) $u_{1/2,1/2}^c = (1 \ 0 \ 0 \ 0 \ 0 \ 0 \ 0 \ 0)^T, \dots, u_{1/2,-1/2}^v = (0 \ 0 \ 0 \ 0 \ 0 \ 0 \ 0 \ 1)^T$ one can rearrange Eq. (16) into the form

$$\begin{aligned} \Psi_{j,m}(\mathbf{r}) &= \sum_{l=j-1/2}^{j+1/2} R_{1/2,l}^{c;j}(r) \mathcal{Y}_{1/2,l}^{c;j,m}(\theta, \phi) \\ &+ \sum_{l=j-3/2}^{j+3/2} R_{3/2,l}^{v;j}(r) \mathcal{Y}_{3/2,l}^{v;j,m}(\theta, \phi) \\ &+ \sum_{l=j-1/2}^{j+1/2} R_{1/2,l}^{v;j}(r) \mathcal{Y}_{1/2,l}^{v;j,m}(\theta, \phi), \end{aligned} \quad (18)$$

where the 8×8 matrices $\mathcal{Y}_{J,l}^{c(v);j,m}(\theta, \phi)$ next to the eight radial envelope functions $R_{J,l}^{c(v);j}(r)$, for a given j , can be found by comparing Eq. (18) with Eqs. (16) and (17). Now, integrating over the angular variables θ and ϕ , it is possible to obtain the radial Hamiltonian

$$\hat{\mathcal{H}}_j = \int (\mathcal{Y}_{J,l}^{b';j,m}(\theta, \phi))^\dagger \hat{H} \mathcal{Y}_{J,l}^{b;j,m}(\theta, \phi) d\Omega, \quad (19)$$

corresponding to the radial Schrödinger equation

$$\sum_{b,J,l} \hat{\mathcal{H}}_j R_{J,l}^{b;j}(r) = E_j R_{J,l}^{b;j}(r), \quad (20)$$

where E_j is the electron or hole eigenenergy to be determined, $b = c$ or v . The Hamiltonian (19) does not depend on m , because within the spherical approximation the energy spectrum is degenerate with respect to the z -component of the total momentum.

After some algebra, we derive the following relations for the spherical harmonics:

$$\begin{aligned} \hat{k}_+ Y_{l,\lambda}(\theta, \phi) &= C_{l+1,\lambda+1;1,-1}^{l,\lambda} B_l^+ Y_{l+1,\lambda+1}(\theta, \phi) \\ &+ C_{l-1,\lambda+1;1,-1}^{l,\lambda} B_l^- Y_{l-1,\lambda+1}(\theta, \phi), \\ \hat{k}_- Y_{l,\lambda}(\theta, \phi) &= -C_{l+1,\lambda-1;1,1}^{l,\lambda} B_l^+ Y_{l+1,\lambda-1}(\theta, \phi) \\ &- C_{l-1,\lambda-1;1,1}^{l,\lambda} B_l^- Y_{l-1,\lambda-1}(\theta, \phi), \end{aligned}$$

$$\begin{aligned}\hat{k}_z Y_{l,\lambda}(\theta, \phi) &= C_{l+1,\lambda;1,0}^{l,\lambda} B_l^+ Y_{l+1,\lambda}(\theta, \phi) \\ &\quad + C_{l-1,\lambda;1,0}^{l,\lambda} B_l^- Y_{l-1,\lambda}(\theta, \phi),\end{aligned}\tag{21}$$

where

$$\begin{aligned}B_l^+ &= -i\sqrt{\frac{l+1}{2l+1}} A_l^{(1)}, \quad B_l^- = -i\sqrt{\frac{l}{2l+1}} A_l^{(-1)}, \\ A_l^{(p)} &= -p \frac{\partial}{\partial r} + \frac{l+1/2-p/2}{r}.\end{aligned}\tag{22}$$

Using the relations (21), the radial Hamiltonian (19) can be obtained in an explicit form. If we choose the following order of the radial functions: $R_{1/2,j-1/2}^{c;j}$, $R_{3/2,j+1/2}^{v;j}$, $R_{3/2,j-3/2}^{v;j}$, $R_{1/2,j+1/2}^{v;j}$, $R_{1/2,j+1/2}^{c;j}$, $R_{3/2,j-1/2}^{v;j}$, $R_{3/2,j+3/2}^{v;j}$, $R_{1/2,j-1/2}^{v;j}$, then the 8×8 matrix of the Hamiltonian $\hat{\mathcal{H}}_j$ takes the form

$$\hat{\mathcal{H}}_j = \begin{pmatrix} \hat{\mathcal{H}}_j^{(1)} & 0 \\ 0 & \hat{\mathcal{H}}_j^{(-1)} \end{pmatrix}.\tag{23}$$

Here, $\hat{\mathcal{H}}_j^{(1)}$ is the 4×4 Hamiltonian of the ‘‘even’’ states and $\hat{\mathcal{H}}_j^{(-1)}$ is the 4×4 Hamiltonian of the ‘‘odd’’ states. It is seen, that the parity p ($p = 1$ for even states and $p = -1$ for odd states) is conserved in the spherical approximation, even when the Hamiltonian is *not* symmetrized. The obtained radial Hamiltonian $\hat{\mathcal{H}}_j^{(p)}$ for the radial functions $R_{1/2,j-p/2}^{c;j}$, $R_{3/2,j+p/2}^{v;j}$, $R_{3/2,j-3p/2}^{v;j}$, and $R_{1/2,j+p/2}^{v;j}$ has the form

$$\hat{\mathcal{H}}_j^{(p)} = \frac{\hbar^2}{2m_0} \begin{pmatrix} \varepsilon_c - \mathcal{T}_{j-p/2} & a_j^p \mathcal{A}_{j+p/2}^{(-p)} & b_j^p \mathcal{A}_{j-3p/2}^{(p)} & p \sqrt{2} \mathcal{A}_{j+p/2}^{(-p)} \\ a_j^p \mathcal{B}_{j-p/2}^{(p)} & \varepsilon_v + \mathcal{P}_{j+p/2}^{(-p)} - c_j^p \mathcal{Q}_{j+p/2}^{(-p)} & a_j^p b_j^p \mathcal{R}_{j-3p/2}^{(p)} & p \sqrt{2} a_j^p \mathcal{Q}_{j+p/2}^{(-p)} \\ b_j^p \mathcal{B}_{j-p/2}^{(-p)} & a_j^p b_j^p \mathcal{R}_{j+p/2}^{(-p)} & \varepsilon_v + \mathcal{P}_{j-3p/2}^{(p)} + c_j^p \mathcal{Q}_{j-3p/2}^{(p)} & p \sqrt{2} b_j^p \mathcal{R}_{j+p/2}^{(-p)} \\ p \sqrt{2} \mathcal{B}_{j-p/2}^{(p)} & p \sqrt{2} a_j^p \mathcal{Q}_{j+p/2}^{(-p)} & p \sqrt{2} b_j^p \mathcal{R}_{j-3p/2}^{(p)} & \varepsilon_v - \delta + \mathcal{P}_{j+p/2}^{(-p)} \end{pmatrix},\tag{24}$$

where $a_j^p = \sqrt{1 + 3\eta_j^p}$, $b_j^p = \sqrt{3(1 - \eta_j^p)}$, $c_j^p = 1 - 3\eta_j^p$, $\eta_j^p = p/(2j + 1 - p)$,

$$\begin{aligned}\mathcal{A}_l^{(p)} &= \frac{1}{2\sqrt{6}} (v_1 A_l^{(p)} + A_l^{(p)} v_2), \\ \mathcal{B}_l^{(p)} &= \frac{1}{2\sqrt{6}} (v_2 A_l^{(p)} + A_l^{(p)} v_1), \\ \mathcal{R}_l^{(p)} &= -A_{l+p}^{(p)} \gamma A_l^{(p)}.\end{aligned}\tag{25}$$

Introducing the operator

$$\Delta_l^{(p)}(\beta) = -A_{l+p}^{(-p)} \beta A_l^{(p)},\tag{26}$$

we can represent \mathcal{T}_l , $\mathcal{P}_l^{(p)}$, and $\mathcal{Q}_l^{(p)}$ as

$$\begin{aligned}\mathcal{T}_l &= \frac{(l+1)\Delta_l^{(1)}(\alpha) + l\Delta_l^{(-1)}(\alpha)}{2l+1}, \\ \mathcal{P}_l^{(p)} &= \frac{(l+1)\Delta_l^{(1)}(\gamma_1 - 2\chi) + l\Delta_l^{(-1)}(\gamma_1 - 2\chi)}{2l+1} + \Delta_l^{(p)}(2\chi), \\ \mathcal{Q}_l^{(p)} &= \frac{(l-1/2)\Delta_l^{(1)}(\gamma - \chi) + (l+3/2)\Delta_l^{(-1)}(\gamma - \chi)}{2l+1} + \Delta_l^{(p)}(\chi).\end{aligned}\tag{27}$$

Inside each spherical layer, the radial Hamiltonian (24) for a spherical QDH coincides with the bulk radial Hamiltonian from Ref. 9 for a spherical QD, when the following denotations for the radial functions are used:

$$\begin{aligned}R_{1/2,j-1/2}^{c;j} &= R_{c,j}^+, & R_{1/2,j+1/2}^{c;j} &= -R_{c,j}^-, \\ R_{3/2,j+1/2}^{v;j} &= R_{h1,j}^+, & R_{3/2,j-1/2}^{v;j} &= R_{h1,j}^-, \\ R_{3/2,j-3/2}^{v;j} &= -R_{h2,j}^+, & R_{3/2,j+3/2}^{v;j} &= -R_{h2,j}^-, \\ R_{1/2,j+1/2}^{v;j} &= R_{s,j}^+, & R_{1/2,j-1/2}^{v;j} &= R_{s,j}^-.\end{aligned}\tag{28}$$

Therefore, in order to find the radial wave functions $R_{J,l}^{c(v);j}$ inside each spherical layer, one can use the same technique as in Ref. 9. When the wave functions inside each spherical layer are known, the BCs should be applied to match the wave functions from two adjacent layers.

IV. BOUNDARY CONDITIONS FOR A SPHERICAL QDH

When considering the multiband models for planar heterostructures, the BCs for the wave function are often obtained by integrating the Schrödinger equation across the heterointerface and assuming the continuity of the wave-function envelopes.^{36,23,19} The resulting BCs are of the following form:

$$\Psi_A|_{z=-0} = \Psi_B|_{z=+0}, \quad \hat{\mathcal{J}}_z \Psi_A|_{z=-0} = \hat{\mathcal{J}}_z \Psi_B|_{z=+0},\tag{29}$$

where A and B are two materials separated by the heterointerface $z = 0$, and $\hat{\mathcal{J}}_z$ is the normal to the heterointerface component of the current operator. The aforementioned integration is actually justified only for Burt's envelope-function equations, because only these have been shown to be valid at the heterointerface. Analogously to the case of planar heterostructures, for spherical QDHs one integrates the radial Schrödinger equation

$$\left(\hat{\mathcal{H}}_j^{(p)} - E_j^{(p)}\right) R_j^{(p)} = 0, \quad R_j^{(p)} = \begin{pmatrix} R_{1/2,j-p/2}^{c;j} \\ R_{3/2,j+p/2}^{v;j} \\ R_{3/2,j-3p/2}^{v;j} \\ R_{1/2,j+p/2}^{v;j} \end{pmatrix},\tag{30}$$

where $\hat{\mathcal{H}}_j^{(p)}$ is defined by Eq. (24) and $E_j^{(p)}$ is the eigenenergy. This integration is carried out across the point $r = a$, where $r = a$ is the spherical heterointerface that separates two materials: A (at $r < a$) and B (at $r > a$). Including the continuity of the radial wave function $R_j^{(p)}$, the required BCs have the form:

$$\begin{aligned} \left(R_j^{(p)}\right)_A \Big|_{r=a-0} &= \left(R_j^{(p)}\right)_B \Big|_{r=a+0}, \\ \hat{\mathcal{J}}_j^{(p)} \left(R_j^{(p)}\right)_A \Big|_{r=a-0} &= \hat{\mathcal{J}}_j^{(p)} \left(R_j^{(p)}\right)_B \Big|_{r=a+0}. \end{aligned} \quad (31)$$

Here the radial component of the current operator $\hat{\mathcal{J}}_j^{(p)}$ is obtained from the radial Hamiltonian $\hat{\mathcal{H}}_j^{(p)}$ using the following procedure. In those terms of the Hamiltonian (24) that contain the operator $A_l^{(p)}$, the utmost left-hand-side $A_l^{(p)}$ is replaced by $-p$ (in conformity with Eq. (22)); the rest of the terms are set to zero; the result is multiplied by $2i/\hbar$. Thus we find

$$\hat{\mathcal{J}}_j^{(p)} = \frac{i\hbar}{m_0} \begin{pmatrix} -\alpha \frac{\partial}{\partial r} & \frac{p}{2\sqrt{6}} a_j^p (v - \xi) & \frac{-p}{2\sqrt{6}} b_j^p (v - \xi) & \frac{1}{2\sqrt{3}} (v - \xi) \\ \frac{-p}{2\sqrt{6}} a_j^p (v + \xi) & \gamma_1 \frac{\partial}{\partial r} - c_j^p \gamma D_r + f_8^{j,p} \frac{\chi}{r} & p a_j^p b_j^p \gamma A_{j-3p/2}^{(p)} & p \sqrt{2} a_j^p \left(\gamma D_r + f_1^{j,p} \frac{\chi}{r} \right) \\ \frac{p}{2\sqrt{6}} b_j^p (v + \xi) & -p a_j^p b_j^p \gamma A_{j+p/2}^{(-p)} & \gamma_1 \frac{\partial}{\partial r} + c_j^p \gamma D_r - 3f_4^{j,p} \frac{\chi}{r} & -\sqrt{2} b_j^p \gamma A_{j+p/2}^{(-p)} \\ \frac{-1}{2\sqrt{3}} (v + \xi) & p \sqrt{2} a_j^p \left(\gamma D_r + f_1^{j,p} \frac{\chi}{r} \right) & \sqrt{2} b_j^p \gamma A_{j-3p/2}^{(p)} & \gamma_1 \frac{\partial}{\partial r} + 2f_{-2}^{j,p} \frac{\chi}{r} \end{pmatrix}, \quad (32)$$

where

$$D_r = \frac{\partial}{\partial r} + \frac{3/2}{r}, \quad f_n^{j,p} = p(j + 1/2 - n p/2). \quad (33)$$

While the radial Hamiltonian $\hat{\mathcal{H}}_j^{(p)}$ is hermitian, the radial component of the current operator $\hat{\mathcal{J}}_j^{(p)}$ is not (as seen from Eq. (32)).

It is important to compare the obtained BCs (31), (32) with the commonly used CRs that the wave function and the normal component of the velocity are continuous at the heterointerface^{11,16}. The velocity operator $\hat{\mathbf{V}}$ is defined as

$$\hat{\mathbf{V}} = \frac{i}{\hbar} [\hat{H}, \mathbf{r}] \equiv \frac{1}{\hbar} \frac{\partial \hat{H}}{\partial \hat{\mathbf{k}}}, \quad (34)$$

where the Hamiltonian \hat{H} has been determined earlier by Eq. (12). Therefore, the normal component of the velocity operator is obtained as follows:

$$\hat{V}_r \equiv \frac{1}{\hbar} \frac{\mathbf{r}}{r} \frac{\partial \hat{H}}{\partial \hat{\mathbf{k}}} = \frac{1}{\hbar} \left(n_+ \frac{\partial \hat{H}}{\partial k_+} + n_- \frac{\partial \hat{H}}{\partial k_-} + n_z \frac{\partial \hat{H}}{\partial k_z} \right), \quad (35)$$

where

$$n_+ = \frac{x + iy}{r\sqrt{2}}, \quad n_- = \frac{x - iy}{r\sqrt{2}}, \quad n_z = \frac{z}{r}. \quad (36)$$

The differentiation of the Hamiltonian can be realized in such a way that

$$\hat{V}_r = \hat{V}_r^L + \hat{V}_r^R, \quad (37)$$

where

$$\hat{V}_r^{L(R)} = \frac{1}{\hbar} \left(n_+ \frac{\partial \hat{H}^{L(R)}}{\partial \hat{k}_+} + n_- \frac{\partial \hat{H}^{L(R)}}{\partial \hat{k}_-} + n_z \frac{\partial \hat{H}^{L(R)}}{\partial \hat{k}_z} \right). \quad (38)$$

Here \hat{H}^L (\hat{H}^R) denotes the Hamiltonian, in which the right(left)-hand operators \hat{k}_+ , \hat{k}_- , and \hat{k}_z are treated as c-numbers, i.e. only the left(right)-hand operators \hat{k}_+ , \hat{k}_- , and \hat{k}_z are differentiated. Using the explicit form of the Hamiltonian \hat{H} (see Eq. (12)), one finds that \hat{V}_r^L can be obtained multiplying by $1/\hbar$ the Hamiltonian \hat{H} , in which all the left-hand operators \hat{k}_+ , \hat{k}_- , and \hat{k}_z are replaced by n_+ , n_- , and n_z , correspondingly, while all the terms that do not contain the former operators are set to zero. It can be also shown that

$$\hat{V}_r^R(\xi, \chi) = \hat{\tau} \hat{V}_r^L(-\xi, -\chi), \quad (39)$$

where the operator $\hat{\tau}$ draws all effective-mass parameters through the operators \hat{k}_+ , \hat{k}_- , and \hat{k}_z to the utmost right-hand positions.

The radial velocity $\hat{\mathcal{V}}_j^{(p),L}$ is obtained from \hat{V}_r^L in the same way as the radial Hamiltonian $\hat{\mathcal{H}}_j^{(p)}$ was obtained from \hat{H} , i.e. by the definition (19). For n_+ , n_- , and n_z (see Eq. (36)) the expressions similar to (21) are valid if one replaces $-i A_l^{(p)}$ by $-p$. Therefore, $\hat{\mathcal{V}}_j^{(p),L}$ can be found by multiplying the Hamiltonian $\hat{\mathcal{H}}_j^{(p)}$ by i/\hbar , replacing all the left-hand operators $A_l^{(p)}$ by $-p$, and setting all the terms, which do not contain the operator $A_l^{(p)}$, to zero. This procedure results in

$$\hat{\mathcal{V}}_j^{(p),L} = \frac{1}{2} \hat{\mathcal{J}}_j^{(p)}, \quad (40)$$

where $\hat{\mathcal{J}}_j^{(p)}$ has been defined by Eq. (32). Using Eqs. (37), (40), and (39) one obtains

$$\hat{\mathcal{V}}_j^{(p)} = \frac{1}{2} \left(\hat{\mathcal{J}}_j^{(p)}(\xi, \chi) + \hat{\tau} \hat{\mathcal{J}}_j^{(p)}(-\xi, -\chi) \right). \quad (41)$$

Considering the explicit form of the matrix $\hat{\mathcal{J}}_j^{(p)}$ we see that all the terms, containing parameters ξ and χ , responsible for the nonsymmetrical form of the Hamiltonian, cancel. Consequently, we obtain

$$\hat{\mathcal{V}}_j^{(p)} = \frac{1 + \hat{\tau}}{2} \hat{\mathcal{J}}_j^{(p)}(\xi = 0, \chi = 0). \quad (42)$$

If all the effective-mass parameters are piecewise-constant functions of r , then at any point of the heterostructure except the spherical heterointerfaces, we can replace $\hat{\tau}$ by 1, and therefore

$$\hat{\mathcal{V}}_j^{(p)} = \hat{\mathcal{J}}_j^{(p)}(\xi = 0, \chi = 0). \quad (43)$$

It is clearly seen now, that the commonly used CRs for spherical QDHs^{11,16} are the same as BCs (31), (32) obtained from the symmetrized Hamiltonian ($\xi = 0, \chi = 0$). Like $\hat{\mathcal{J}}_j^{(p)}$, the radial component of the velocity operator (42) is not hermitian when $\hat{\tau} = 1$. Therefore, in order to prove that both current and velocity are conserved simultaneously, we should verify whether the real parts of the current density and of the velocity density are the same, i.e. we should check whether the equality

$$\text{Re} \left[\left(R_j^{(p)} \right)^\dagger \hat{\mathcal{J}}_j^{(p)} R_j^{(p)} \right] = \text{Re} \left[\left(R_j^{(p)} \right)^\dagger \hat{\mathcal{V}}_j^{(p)} R_j^{(p)} \right] \quad (44)$$

holds true. Here $R_j^{(p)}$ is the radial wave function defined by Eq. (30). Substituting Eq. (32) into the left-hand-side part of Eq. (44), we see that all the terms containing the parameters ξ and χ cancel, because their contribution to the current density is purely imaginary. Therefore, in conformity with Eq. (43), the equation (44) is proven to be fair.

V. RESULTS OF THE CALCULATION AND DISCUSSION

In this section we investigate the electronic structure of three spherical QDHs with different values of the energy gaps: a zero-gap semiconductor embedded into a wide-gap semiconductor (HgS/CdS), a narrow-gap semiconductor embedded into a medium-gap semiconductor (InAs/GaAs), and a medium-gap semiconductor embedded into a wide-gap semiconductor (GaAs/AlAs). Note that in these widely used experimentally relevant materials, the effective-mass parameters are substantially different. The bulk 8-band parameters of the used III-V and IV-VI materials are listed in Tables I and II, correspondingly. For electron and hole levels, obtained within the spherical 8-band model, we use a common notation: $nQ_j^{(e)}$ denotes an electron state and $nQ_j^{(h)}$ denotes a hole state, where n is the number of the level with a given symmetry and $Q = S, P, D, \dots$ denotes the lowest value of the momentum l in the spherical harmonics of Eq. (18) in front of the CB Bloch functions for an electron state and in front of the VB Bloch functions for a hole state, i.e. $Q = j - p/2$ for an electron and $Q = \min(j + p/2, |j - 3p/2|)$ for a hole.

A. Electron energy levels

The electron energy levels of the HgS/CdS, InAs/GaAs, and GaAs/AlAs QDHs are depicted in Figs. 1-3, correspondingly, as a function of the quantum dot radius a . The value of the spin-orbit splitting of electron energy levels is small (≈ 3 meV) for all considered QDHs (see Table III and Appendix B). Therefore, only the lowest level of the pair of split levels is shown in Figs. 1-3. For all examined QDHs, the lowest level of such a pair is the level with the least total momentum j .

Analyzing Figs. 1-3 we arrive at the following empirical formula, which determines the energy shift of all electron levels with $n = 1$ when a nonzero value of the parameter χ is considered:

$$E_e - E_e|_{\chi=0} = -\frac{\hbar^2}{m_0 a^2}(\chi_1 - \chi_2). \quad (45)$$

Here the indices “1” and “2” denote interior and exterior materials, correspondingly. For $n > 1$ the value of this shift is much smaller, than for $n = 1$. It is seen that the shift $E_e - E_e|_{\chi=0}$ is about 16 meV for HgS/CdS ($a = 2$ nm) and about 4 meV for InAs/GaAs ($a = 4$ nm) and GaAs/AlAs ($a = 3$ nm) QDHs (see Table III). As provided by Eq. (45), the value of this shift is inversely proportional to the square of the quantum dot radius. Consequently, for large QDHs one can use with high accuracy the symmetrized with respect to χ Hamiltonian, and the expression (45) is the measure of accuracy. If $\chi_1 < \chi_2$, then the nonsymmetrized energy level lies higher than the symmetrized one (see Figs. 1, 3), and if $\chi_1 > \chi_2$, then the nonsymmetrized energy level lies lower than the symmetrized one (see Fig. 2).

Gray bands in Figs. 1-3 reflect the change of the parameter c_ξ (see Eq. (8)) from 1 to -1 . The chosen interval includes the following specific values of c_ξ : $c_\xi = 0$ (symmetrized Hamiltonian) and $c_\xi = \pm 1$ (see Appendixes A and B). With such a change of c_ξ , the electron energy increases in Figs. 1, 2 and decreases in Fig. 3. Therefore, the shift of an energy level with $n = 1$ with respect to the level position when $c_\xi = 0$ can be estimated by the formula:

$$E_e - E_e|_{c_\xi=0} = b c_\xi \left(\sqrt{E_{p,1}} - \sqrt{E_{p,2}} \right) \quad (b > 0), \quad (46)$$

where we take into account Eq. (8) and the fact that $v_{1,2} \sim \sqrt{E_{p,1,2}}$. E_p is the Kane energy (see Tables I and II). For $n > 1$ the shift $E_e - E_e|_{c_\xi=0}$ becomes much smaller, than for $n = 1$. The parameter b in Eq. (46) decreases with increasing a and with increasing the energy gap in the interior material. Such a behaviour of the parameter b is connected with the fact that it is proportional to the value of hole radial components of the electron wave function at the heterointerface. It is clear now that the observed strong dependence of the energy levels in the HgS/CdS QDH on c_ξ (see Fig. 1) is due to the large value of the difference $\sqrt{E_{p,1}} - \sqrt{E_{p,2}}$ and to the zero energy gap in HgS. For two other QDHs the dependence of the energy levels on c_ξ is a few times weaker, than that for the HgS/CdS QDH.

Hence, Eqs. (45) and (46) allow us to estimate corrections to the eigenenergies due to the replacement of the heuristic symmetrized Hamiltonian with the nonsymmetrized Hamiltonian avoiding complicated calculations. It follows from Eq. (45) that such corrections rise with decreasing the quantum dot radius as $1/a^2$. Therefore, one should use the nonsymmetrized Hamiltonian for description of quantum dots with small radii.

B. Hole energy levels

All the hole energy levels of S - and P -types in the HgS/CdS QDH, with $j = 3/2$ in the InAs/GaAs QDHs and with $j = 3/2$ in the GaAs/AlAs QDHs are depicted in Figs. 4, 5 and 6, correspondingly, as a function of the quantum dot radius. It is seen from these figures that the empirical formula (45) holds for hole levels, too, i.e. for a nonzero value of χ , the hole energy levels shift in the same direction as the electron energy levels do. For the HgS/CdS QDH ($a = 2$ nm) the shift of the hole ground state level is about 9 meV, what is smaller than the shift of the electron ground state level. At the same time, for InAs/GaAs

($a = 4$ nm) and GaAs/AlAs ($a = 3$ nm) QDHs the shift for the hole ground state level is almost the same as that for the electron ground state level (see Table III). For the higher hole levels ($n > 1$) the value of the shift under consideration decreases with increasing n much weaker than it does for the electron levels.

The dependence of the hole levels on the parameter c_ξ is substantially different from such a dependence for the electron levels. The formula (46) can be approximately applied here only for the level $1S_{3/2}^{(h)}$, which is the hole ground state energy for all examined QDHs. It is seen that this energy level strongly depends on c_ξ even for InAs/GaAs and GaAs/AlAs QDHs. All the other hole energy levels under analysis depend on c_ξ very weakly, and such a dependence is revealed only in Fig. 4 for the HgS/CdS QDH.

C. Electron and hole wave functions and pair energies

In Figs. 7, 8, and 9, the S -components of the radial wave functions of the electron ground state ($1S_{1/2}^{(e)}$) and of the hole ground state ($1S_{3/2}^{(h)}$) are depicted for HgS/CdS ($a = 2$ nm), InAs/GaAs ($a = 4$ nm), and GaAs/AlAs ($a = 3$ nm) QDHs, correspondingly. It is seen that in all these QDHs, the hole density in the interior material is higher than the electron density, and the electron density is higher in the exterior material. It is also seen that when c_ξ changes from 1 to -1 , the electron density in the centers of the HgS/CdS and InAs/GaAs QDHs increases and the hole density decreases. The opposite trends of behavior of the electron and hole densities are observed in the center of the GaAs/AlAs QDH. The abrupt change of the derivative of the electron radial component with the change of c_ξ is well seen at the heterointerfaces of all QDHs under consideration. At the same time, the derivative of the hole radial component changes smoothly. The contribution of the hole radial components to the density of the electron state (at $c_\xi=0$) is as high as 33 % for HgS/CdS, 20 % for InAs/GaAs, and 14 % for GaAs/AlAs QDH. Such contributions show that the nonparabolicity of the electron dispersion law is substantial even for the QDs of the medium-gap semiconductors (GaAs) and certainly should be taken into consideration when the QDs of the narrow-gap semiconductors (InAs) are investigated. The contribution of the electron radial component to the density of the hole state (at $c_\xi=0$) is 6 % for HgS/CdS, 1 % for InAs/GaAs, and 1 % for GaAs/AlAs QDH. This fact leads to the conclusion that the additional nonparabolicity of the hole dispersion law connected with the influence of the conduction band can be neglected for both narrow- and medium-gap semiconductor QDs.

Taking into account the principal role of the dissymmetry coefficient c_ξ , one can evaluate the influence of this parameter on the observable effects. With this purpose we calculate the lowest electron-hole pair energies as a function of c_ξ for all QDHs under consideration (see Fig. 10). It is seen from Fig. 10 that when the parameter c_ξ changes from -2 to 2 , the corresponding energy differences $E_{e-h}(c_\xi = 2) - E_{e-h}(c_\xi = -2)$ constitute -175 meV for HgS/CdS ($a = 2$ nm), -15 meV for InAs/GaAs ($a = 4$ nm), and 20 meV for GaAs/AlAs ($a = 3$ nm) QDHs. These differences should be quite accessible for the experimental detection.

VI. CONCLUSIONS

The exact nonsymmetrized 8-band effective-mass Hamiltonian for an arbitrary 3-dimensional heterostructure has been obtained using the Burt's envelope-function representation. The 2×2 electron and 6×6 hole energy-dependent Hamiltonians have been deduced. Within the spherical approximation, the 8×8 , 2×2 , and 6×6 radial Hamiltonians and the necessary BCs have been derived for spherical QDHs. The boundary conditions for radial symmetrized and nonsymmetrized Hamiltonians are different and lead therefore to different energy levels and wave functions. We have shown, further, that the CRs, which are commonly used to match the solutions of the appropriate bulk $\mathbf{k} \cdot \mathbf{p}$ Hamiltonians, coincide with BCs for the symmetrized Hamiltonians. A theoretical estimate for the value of the spin-orbit splitting of electron levels has been found. The energy levels of the nonsymmetrized 8-band Hamiltonian have been calculated as a function of the dot radius for three spherical QDHs: a zero-gap semiconductor embedded into a wide-gap semiconductor (HgS/CdS), a narrow-gap semiconductor embedded into a medium-gap semiconductor (InAs/GaAs), and a medium-gap semiconductor embedded into a wide-gap semiconductor (GaAs/AlAs). It has been demonstrated that parameters of dissymmetry $\chi(\mathbf{r})$ and $\xi(\mathbf{r})$, giving nonzero contribution to the multiband Hamiltonians only at the heterointerfaces, have, nevertheless, a strong effect on the electron and hole spectra. Thus, for practically important cases of relatively small QDHs with noticeably different effective-mass parameters of the constituent materials, the use of the obtained Hamiltonian is necessary for the adequate description of experiment.

ACKNOWLEDGEMENTS

This work has been supported by the GOA BOF UA 2000, IUAP, FWO-V projects G.0287.95, G.0274.01N and the W.O.G. WO.025.99N (Belgium).

APPENDIX A: INTERBAND MOMENTUM MATRIX ELEMENTS

Using the general effective mass equations [Eq. (6.3) of Ref. 19], one can see the origin of the interband momentum matrix elements $v_1(\mathbf{r})$ and $v_2(\mathbf{r})$ from Eq. (1):

$$v_1(E, \mathbf{r}) = -\frac{4i}{\hbar} \langle S | \hat{p}_z | Z \rangle - \frac{4i}{\hbar} \sum_{\nu} (E - H_{\nu\nu}(\mathbf{r}))^{-1} H_{S\nu}(\mathbf{r}) \langle \nu | \hat{p}_z | Z \rangle; \quad (\text{A1})$$

$$v_2(E, \mathbf{r}) = -\frac{4i}{\hbar} \sum_{\nu} (E - H_{\nu\nu}(\mathbf{r}))^{-1} \langle S | \hat{p}_z | \nu \rangle H_{\nu Z}(\mathbf{r}). \quad (\text{A2})$$

To obtain Eqs. (A1) and (A2) it should be taken into account that within the developed 8-band approach the conduction band with the Bloch function $|S\rangle$ and the valence band with the Bloch functions $|X\rangle$, $|Y\rangle$, and $|Z\rangle$ are included explicitly, while all other bands with the Bloch functions $|\nu\rangle$ are considered to be remote. Further, following the technique of Ref. 19 it is necessary to exclude the energy dependence from Eqs. (A1) and (A2) by replacing E

with an average energy, for instance the energy at the middle of the narrowest gap for the heterostructure compounds. Parameters $v_1(\mathbf{r})$ and $v_2(\mathbf{r})$ are approximately considered to be constant in each layer of a heterostructure.

In bulk, if Burt's material-independent basis functions coincide with the bulk Bloch functions, the second term in the r.h.s. of Eq. (A1) and the r.h.s. of Eq. (A2) vanish, because in this case $H_{S\nu}(\mathbf{r}) = 0$ and $H_{\nu Z}(\mathbf{r}) = 0$. Therefore, one obtains $v_1 = 2v$ ($v = -2i\langle S|\hat{p}_z|Z\rangle/\hbar$) and $v_2 = 0$, what results in $\xi = v$ (see Eq. (2)) and $c_\xi = 1$ (see Eq. (8)). When materials constituting the heterostructure have close parameters, the second term in the r.h.s. of Eq. (A1) and the r.h.s. of Eq. (A2) are small compared with the first term in the r.h.s. of Eq. (A1). In this case ξ does not differ significantly from v , and c_ξ is close to 1. In a general case of disparate materials, c_ξ can take arbitrary values.

APPENDIX B: ENERGY-DEPENDENT SEPARATE HAMILTONIANS FOR ELECTRONS AND HOLES

For narrow-gap semiconductors, the accurate way to take into account the coupling of conduction and valence bands, is to consider the 8-band Hamiltonian. However, sometimes it is easier to solve a CB or VB Schrödinger equation with energy-dependent effective-mass parameters. Solutions of these equations are just an approximation to the results of the 8-band model. In what follows, we deduce the 2×2 energy-dependent Hamiltonian for an electron and the 6×6 energy-dependent Hamiltonian for a hole from the exact 8-band nonsymmetrized effective mass Hamiltonian.

1. 2×2 energy-dependent Hamiltonian for an electron

a. Nonsymmetrized CB Hamiltonian

We start with the nonsymmetrized 8-band Hamiltonian \hat{H} defined by Eq. (12). The wave function Ψ , i.e. a vector of eight envelope functions Ψ_1, \dots, Ψ_8 is an eigenfunction of the matrix Schrödinger equation

$$\hat{H}\Psi = E\Psi, \tag{B1}$$

where E is an eigenenergy. To find the CB Hamiltonian, one should treat all VBs as remote. Therefore, we should exclude all VB envelopes, i.e. Ψ_3, \dots, Ψ_8 , from Eq. (B1). As seen, this exclusion is possible only within the approximation $\gamma_1 = 0$, $\gamma_2 = 0$, and $\gamma_3 = 0$, in other words, when the contributions to the hole effective-mass parameters from the remote bands (all bands except two CBs and six VBs) is negligible. This is a very close approximation, because the parameters γ_1 , γ_2 , and γ_3 are small for almost all materials and, determining contributions to the VB, they certainly have small influence on the electron levels. Under this approximation $\chi = -1/3$ (see Eq. (7)) and it cancels from the Hamiltonian. Another necessary approximation is $c_\xi = -1$, i.e. $\xi = -v$, and therefore $v_1 = 0$, $v_2 = 2v$ (see Eqs. (8) and (2)). This is the only approximation that does not lead to the discontinuity of CB envelopes Ψ_1 and Ψ_2 at the heterointerface. Now we can express six VB envelopes $\Psi_3, \dots,$

Ψ_8 in terms of two CB envelopes Ψ_1 and Ψ_2 using the last six equations of the set (B1). This procedure results in

$$\begin{aligned}
\Psi_3 &= -i \frac{v}{\varepsilon - \varepsilon_v} \hat{k}_- \Psi_1, \\
\Psi_4 &= \frac{v}{\varepsilon - \varepsilon_v} \left(\sqrt{\frac{2}{3}} \hat{k}_z \Psi_1 - \frac{1}{\sqrt{3}} \hat{k}_- \Psi_2 \right), \\
\Psi_5 &= \frac{v}{\varepsilon - \varepsilon_v} \left(\frac{-i}{\sqrt{3}} \hat{k}_+ \Psi_1 - i \sqrt{\frac{2}{3}} \hat{k}_z \Psi_2 \right), \\
\Psi_6 &= -\frac{v}{\varepsilon - \varepsilon_v} \hat{k}_+ \Psi_2, \\
\Psi_7 &= \frac{v}{\varepsilon - \varepsilon_v + \delta} \left(\frac{-i}{\sqrt{3}} \hat{k}_z \Psi_1 - i \sqrt{\frac{2}{3}} \hat{k}_- \Psi_2 \right), \\
\Psi_8 &= \frac{v}{\varepsilon - \varepsilon_v + \delta} \left(\sqrt{\frac{2}{3}} \hat{k}_+ \Psi_1 - \frac{1}{\sqrt{3}} \hat{k}_z \Psi_2 \right),
\end{aligned} \tag{B2}$$

where $\varepsilon = 2m_0E/\hbar^2$. Substituting the envelopes (B2) into the first two equations of the set (B1), one obtains the sought CB Hamiltonian for the electron envelopes Ψ_1 and Ψ_2 . This Hamiltonian has the form

$$\hat{H}_e = \frac{\hbar^2}{2m_0} \begin{pmatrix} \varepsilon_c + P_e & C_e \\ C_e^\dagger & \varepsilon_c + P_e^* \end{pmatrix}, \tag{B3}$$

where

$$\begin{aligned}
P_e &= \hat{k}_+ \left(\frac{m_0}{m_c(\varepsilon)} + g_c(\varepsilon) \right) \hat{k}_- + \hat{k}_- \left(\frac{m_0}{m_c(\varepsilon)} - g_c(\varepsilon) \right) \hat{k}_+ + \hat{k}_z \frac{m_0}{m_c(\varepsilon)} \hat{k}_z, \\
C_e &= -\sqrt{2} \left(\hat{k}_z g_c(\varepsilon) \hat{k}_- - \hat{k}_- g_c(\varepsilon) \hat{k}_z \right),
\end{aligned} \tag{B4}$$

$$\begin{aligned}
\frac{m_0}{m_c(\varepsilon)} &= \alpha + \frac{v^2}{3} \left(\frac{2}{\varepsilon - \varepsilon_v} + \frac{1}{\varepsilon - \varepsilon_v + \delta} \right), \\
g_c(\varepsilon) &= \frac{v^2}{3} \left(\frac{1}{\varepsilon - \varepsilon_v} - \frac{1}{\varepsilon - \varepsilon_v + \delta} \right).
\end{aligned} \tag{B5}$$

Here, $m_0/m_c(\varepsilon)$ is the inverse of the energy-dependent effective mass of an electron, and $g_c(\varepsilon)$ is an energy-dependent interfacial parameter, which vanishes when the spin-orbit splitting δ is zero. Like χ , this parameter gives a nonzero contribution to the Hamiltonian only at the heterointerface. The parameter $g_c(\varepsilon)$ is responsible for the nonsymmetrical form of the Hamiltonian (B3) and for the mixing of the envelopes Ψ_1 and Ψ_2 . When one solves the Schrödinger equation for an electron using the energy-dependent Hamiltonian (B3), one finds the eigenenergy E and eigenfunctions Ψ_1 and Ψ_2 . Then, substituting these eigenfunctions into Eq. (B2), one obtains the rest envelopes Ψ_3, \dots, Ψ_8 , and therefore Ψ . While the functions Ψ_1 and Ψ_2 are continuous at the heterointerface, the functions Ψ_3, \dots, Ψ_8 , as the envelope functions of all the other remote bands, are not.¹⁹ Note, that only the wave functions

Ψ , i.e. vectors of eight envelope functions Ψ_1, \dots, Ψ_8 are orthonormalized. The envelopes Ψ_1 and Ψ_2 are neither orthogonal nor properly normalized. When the nonparabolicity is not strong, in other words, when $m_c(\varepsilon)$ only weakly depends on the energy, it is possible to choose one appropriate value of the energy, e. g. ε_0 , to find $m_c(\varepsilon_0)$ and $g_c(\varepsilon_0)$, and to substitute them into the Hamiltonian (B3). In such a way one obtains the Hamiltonian $\hat{H}_c(\varepsilon_0)$. The eigenfunctions Ψ_1 and Ψ_2 of this Hamiltonian will be orthonormalized and the rest six envelopes will be no longer needed.

b. CB Hamiltonian and BCs for a spherical QDH

The radial CB Hamiltonian $\hat{\mathcal{H}}_{e,j}^{(p)}$ for spherical QDHs can be derived from the Hamiltonian (B3) by the same way as the radial Hamiltonian (24) has been obtained from the Hamiltonian (12) in the spherical approximation (see Sec. III). Thus we find

$$\hat{\mathcal{H}}_{e,j}^{(p)} = \frac{\hbar^2}{2m_0} \left(\varepsilon_c - \mathcal{P}_{e,j-p/2}^{(p)} \right), \quad (\text{B6})$$

where

$$\mathcal{P}_{e,l}^{(p)} = \frac{(l+1)\Delta_l^{(1)} \left(\frac{m_0}{m_c(\varepsilon)} + g_c(\varepsilon) \right) + l\Delta_l^{(-1)} \left(\frac{m_0}{m_c(\varepsilon)} + g_c(\varepsilon) \right)}{2l+1} - \Delta_l^{(p)}(g_c(\varepsilon)) \quad (\text{B7})$$

and the operator $\Delta_l^{(p)}(\beta)$ is defined by Eq. (26). Inside the i -th spherical layer, the Hamiltonian (B6) takes the form

$$\hat{\mathcal{H}}_{e,j}^{i,(p)} = \frac{\hbar^2}{2m_0} \left(\varepsilon_c - \frac{m_0}{m_{c,i}(\varepsilon)} \Delta_{j-p/2} \right), \quad (\text{B8})$$

where Δ_l is the spherical Laplacian and $m_{c,i}(\varepsilon)$ is the energy-dependent CB mass of the i -th material. Further, one should solve the Schrödinger equation with the Hamiltonian (B8) for each spherical layer and match the obtained solutions at the spherical heterointerfaces using the BCs (31) (see Sec. IV). The radial component of the CB current operator $\hat{\mathcal{J}}_{e,j}^{(p)}$ is obtained from the Hamiltonian (B6) by the same way as the radial component of the current operator (32) has been obtained from the Hamiltonian (24). Thus,

$$\hat{\mathcal{J}}_{e,j}^{(p)} = \frac{i\hbar}{m_0} \left(-\frac{m_0}{m_c(\varepsilon)} \frac{\partial}{\partial r} - p(j+1/2-p) \frac{g_c(\varepsilon)}{r} \right). \quad (\text{B9})$$

In a two-layer spherical QDH the electron energy depends on the difference $g_{c,1}(\varepsilon) - g_{c,2}(\varepsilon)$ (as seen from the BCs (31), (B9)), where the indices “1” and “2” denote the interior and exterior materials, correspondingly. The value of this difference is usually very small for typical QDHs. Therefore, in the first approximation, one can find the energy spectrum E_l ($l = j - p/2$) neglecting the term proportional to $p(j+1/2-p)(g_{c,1}(\varepsilon) - g_{c,2}(\varepsilon))$ in the BCs. Then, including this term as a perturbation, one finds the energy spectrum E_l^j . It is seen that the energy levels with $l = 0$ remain unchanged, while each energy level E_l with $l \geq 1$ splits into two levels: $E_l^{l+1/2}$ and $E_l^{l-1/2}$. For the electron levels that are not very close to

the CB minimum (it is the case for the QDHs under consideration), the following estimate can be obtained

$$E_l = \frac{(l+1)E_l^{l+1/2} + lE_l^{l-1/2}}{2l+1}, \quad E_l^{l+1/2} - E_l^{l-1/2} = \frac{\hbar^2(2l-1)}{m_0a^2} (g_{c,1}(\varepsilon_l) - g_{c,2}(\varepsilon_l)), \quad (\text{B10})$$

where $\varepsilon_l = 2m_0E_l/\hbar^2$. In Table III we have used Eq. (B10) to estimate the spin-orbit splitting of the lowest P and D levels. It is seen that the value of the splitting of the electron levels is of the order of 3 meV in all considered QDHs, and therefore this splitting can be neglected. This fact does not imply that the dependence of the parameters of the CB Hamiltonian on the energy can be neglected, too. As seen from Table III, the electron effective masses in QDHs can differ by a factor of 2 from their values in the corresponding bulk materials.

2. 6×6 energy-dependent Hamiltonian for a hole

a. Nonsymmetrized VB Hamiltonian

The deduction of the VB Hamiltonian is analogous to the deduction of the CB Hamiltonian with the only difference: one should treat two CBs as remote. In order to express the CB envelopes Ψ_1 and Ψ_2 in terms of the VB envelopes Ψ_3, \dots, Ψ_8 and to exclude them from the Schrödinger equation (B1), one should apply the approximation $\alpha = 0$ and $c_\xi = 1$. This approximation has the same grounds as the approximation used above to obtain the CB Hamiltonian. Now, we express the CB envelopes Ψ_1 and Ψ_2 in terms of the VB envelopes Ψ_3, \dots, Ψ_8 from the first two equations of the set (B1) and substitute them into the last six equations of the same set. As a result we have the VB Hamiltonian \hat{H}_h , which coincides with the Hamiltonian \hat{H} (see Eq. (12)) where the first two rows and the first two columns are deleted and the effective-mass parameters are changed in the following way:

$$\begin{aligned} \gamma_1 &\rightarrow \gamma_1^L(\varepsilon) = \gamma_1 + \frac{v^2}{3(\varepsilon_c - \varepsilon)}, \\ \gamma_{2,3} &\rightarrow \gamma_{2,3}^L(\varepsilon) = \gamma_{2,3} + \frac{v^2}{6(\varepsilon_c - \varepsilon)}. \end{aligned} \quad (\text{B11})$$

Here, $\gamma_i^L(\varepsilon)$ are the energy-dependent Luttinger parameters. In conformity with Eq. (7), one should change the parameter of dissymmetry χ as follows

$$\chi \rightarrow \chi^L(\varepsilon) = \chi + \frac{v^2}{6(\varepsilon_c - \varepsilon)}. \quad (\text{B12})$$

As a result of the change (B12), the parameter of dissymmetry increases (see Table III), therefore the results of the symmetrized Hamiltonian (with $\chi^L = 0$) will deviate sharply from the exact solutions. The parameters γ_i^L usually weakly depend on the energy. Consequently, to obtain the hole spectrum one can use the Hamiltonian $\hat{H}_h(\varepsilon_0)$, where ε_0 is an average hole energy.

b. VB Hamiltonian and BCs for a spherical QDH

The radial VB Hamiltonian $\hat{\mathcal{H}}_{h,j}^{(p)}$ for a spherical QDH coincides with the radial Hamiltonian (24) in which $\gamma_1 \rightarrow \gamma_1^L(\varepsilon)$ and $\chi \rightarrow \chi^L(\varepsilon)$ (in conformity with Eqs. (B11) and (B12)), $\gamma \rightarrow \gamma^L(\varepsilon) = \gamma + \frac{v^2}{6(\varepsilon_c - \varepsilon)}$ (in conformity with Eqs. (B11) and (14)) and where the first two rows and the first two columns are deleted. For the radial components of the hole wave function one should use the BCs (31), in which the radial component of the current operator $\hat{\mathcal{J}}_{h,j}^{(p)}$ is given by the matrix (32) where the first row and the first column are deleted and the parameters γ_1, γ, χ are replaced by the parameters $\gamma_1^L, \gamma^L, \chi^L$, correspondingly.

TABLES

TABLE I. The 8-band effective-mass parameters of some III-V materials. The VB offset E_v is chosen to be zero in GaAs. The parameters α , γ_1 , γ , and χ of the spherical model are calculated from the listed here effective-mass parameters.

Parameters	GaAs	AlAs	InAs
$m_c (m_0)$	0.0665 ^c	0.150 ^c	0.02226 ^a
γ_1^L	7.10 ^d	3.76 ^d	19.67 ^c
γ_2^L	2.02 ^d	0.90 ^d	8.37 ^c
γ_3^L	2.91 ^d	1.42 ^d	9.29 ^c
E_p (eV)	28.0 ^b	21.1 ^c	22.2 ^c
E_g (eV)	1.519 ^c	3.130 ^c	0.418 ^c
Δ (eV)	0.341 ^c	0.275 ^c	0.380 ^c
E_v (eV)	0	-0.532 ^d	0.186 ^e
α	-2.27	0.11	0.24
γ_1	0.96	1.51	1.97
γ	-0.52	0.09	0.07
χ	-1.52	-0.69	-0.87

^aRef. 37

^bRef. 38

^cRef. 39

^dRef. 40

^eRef. 13

TABLE II. The 8-band effective-mass parameters of some IV-VI materials. The VB offset E_v is chosen to be zero in HgS. The parameters of the spherical model α , γ_1 , γ , and χ for CdS and χ for HgS are calculated from the listed here effective-mass parameters. The parameters m_c , γ_1^L , and γ^L are not presented for HgS, because in a semimetal the band structure is inverted and these parameters do not have their original sense.

Parameters	HgS	CdS
$m_c (m_0)$	–	0.18 ^f
γ_1^L	–	1.71 ^f
γ^L	–	0.62 ^f
E_p (eV)	13.2 ^a	21.0 ^e
E_g (eV)	–0.190 ^a	2.56 ^c
Δ (eV)	0.07 ^c	0.07 ^c
E_v (eV)	0	–0.93 ^d
α	–1.0 ^c	–2.57
γ_1	0.35 ^b	–1.02
γ	–0.67 ^b	–0.75
χ	–1.57	–1.24

^aRef. 41

^bRef. 42

^cRef. 44

^dRef. 45

^eRef. 46

^fRef. 47

TABLE III. The spin-orbital splitting of electron energy levels ($c_\xi = -1$); the energy-dependent electron effective masses ($c_\xi = -1$); the energy shift of electron and hole levels due to finite values of χ (at $c_\xi = 0$); and the difference of χ^L in adjacent materials for the 6×6 model (at $c_\xi = 1$). If not indicated explicitly, $\chi \neq 0$. E_e and E_h are the electron and hole ground state energies corresponding to the states $1S_{1/2}^{(e)}$ and $1S_{3/2}^{(h)}$. The indices “1” and “2” denote the interior and exterior materials, correspondingly.

	HgS/CdS	InAs/GaAs	GaAs/AlAs
	$a = 2$ nm	$a = 4$ nm	$a = 3$ nm
$E_{1P_{3/2}^{(e)}} - E_{1P_{1/2}^{(e)}}$ (meV) ^a	2.6 (2.0)	3.0 (1.4)	2.7 (3.0)
$E_{1D_{5/2}^{(e)}} - E_{1D_{3/2}^{(e)}}$ (meV) ^a	2.0 (2.3)	3.8 (2.2)	4.5 (7.1)
$m_{c,1}(E_e)$ (m_0) ^b	0.056 (–)	0.038 (0.022)	0.083 (0.067)
$m_{c,2}(E_e)$ (m_0) ^b	0.097 (0.180)	0.040 (0.067)	0.115 (0.150)
$E_e - E_e _{\chi=0}$ (meV) ^c	16.1 (6.3)	–3.5 (–3.1)	4.8 (7.0)
$E_h - E_h _{\chi=0}$ (meV) ^c	9.3 (6.3)	–4.1 (–3.1)	4.1 (7.0)
$\chi_1^L(E_h) - \chi_2^L(E_h)$ ^d	36.28 (–0.33)	4.86 (0.65)	0.73 (–0.83)

^aThe theoretical estimate based on the 2×2 energy-dependent Hamiltonian for an electron (see Appendix B) is given in parentheses.

^bThe corresponding bulk effective mass (see Tables I and II) is given in parentheses.

^cThe result of the empirical estimate $E_{e(h)} - E_{e(h)}|_{\chi=0} = -\frac{\hbar^2}{m_0 a^2}(\chi_1 - \chi_2)$ is given in parentheses.

^dThe difference $\chi_1 - \chi_2$ for the 8-band model (see Tables I and II) is given in parentheses.

FIGURES

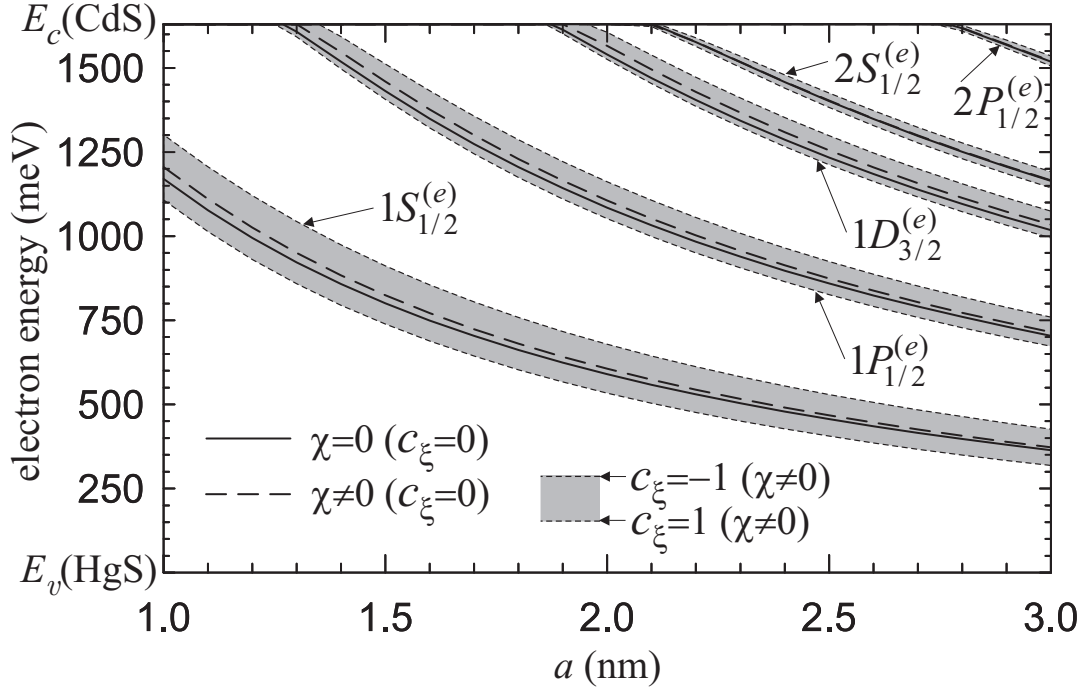


FIG. 1. All the discrete electron energy levels in the HgS/CdS QDH as a function of the quantum dot radius. The $P_{3/2}^{(e)}$ and $D_{5/2}^{(e)}$ energy levels are not shown here and in Figs. 2 and 3 because in the chosen scale they coincide with the levels $P_{1/2}^{(e)}$ and $D_{3/2}^{(e)}$, correspondingly. Solid lines represent the result of the symmetrized 8-band model ($c_\xi = 0$, $\chi = 0$). With the nonsymmetrized valence band part of the Hamiltonian ($\chi \neq 0$), dashed lines show the case $c_\xi = 0$ while gray bands represent the continuous change of c_ξ from 1 to -1 . The gray bands refer to a possible variation in energy due to conduction band/valence band coupling via the position dependence of the interband momentum matrix element. Here and in Figs. 2 - 6, the insert with inscriptions $c_\xi = -1$ and $c_\xi = 1$ shows to which values of c_ξ the edges of the gray bands are related.

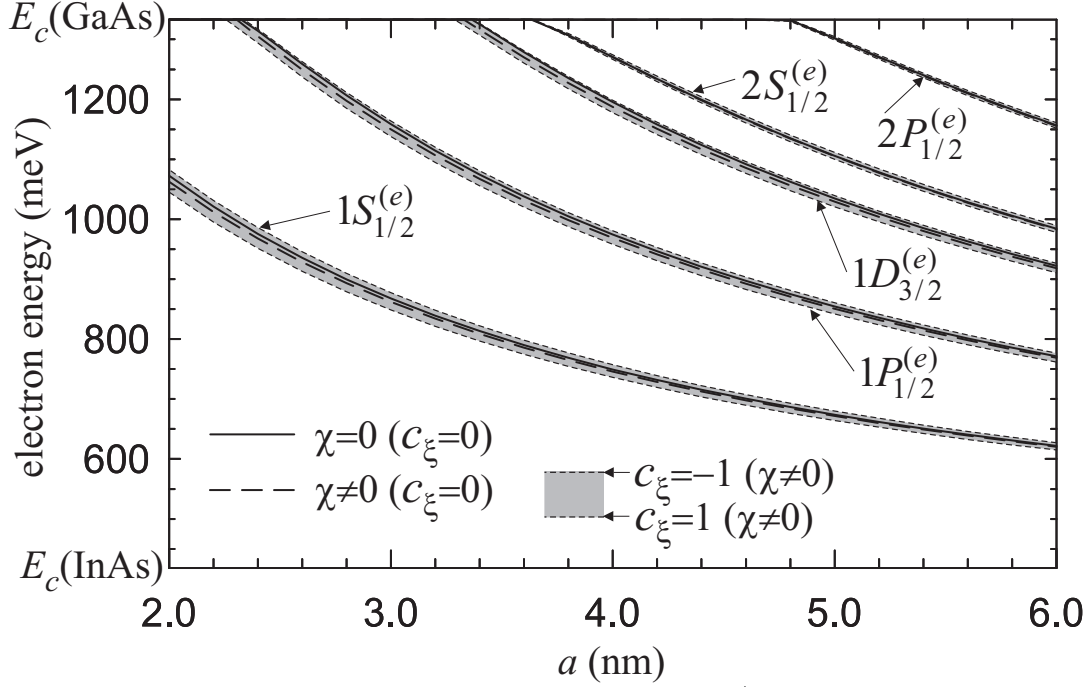


FIG. 2. All the discrete electron energy levels in the InAs/GaAs QDH as a function of the quantum dot radius. Other denotations are the same as in Fig. 1.

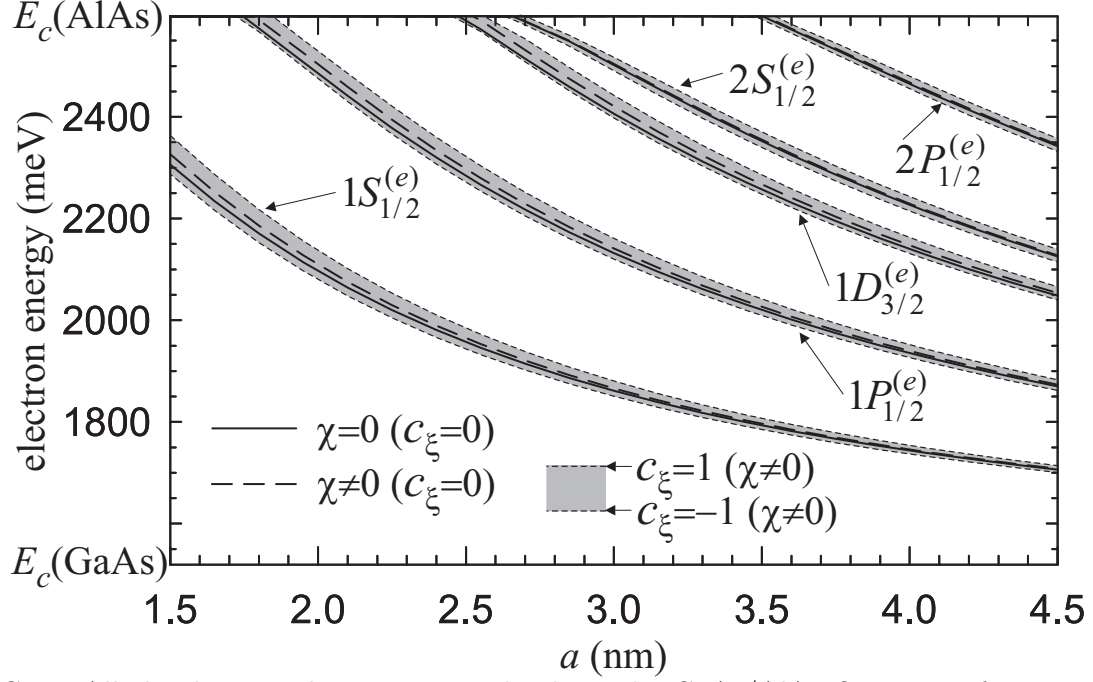


FIG. 3. All the discrete electron energy levels in the GaAs/AlAs QDH as a function of the quantum dot radius. Other denotations are the same as in Fig. 1.

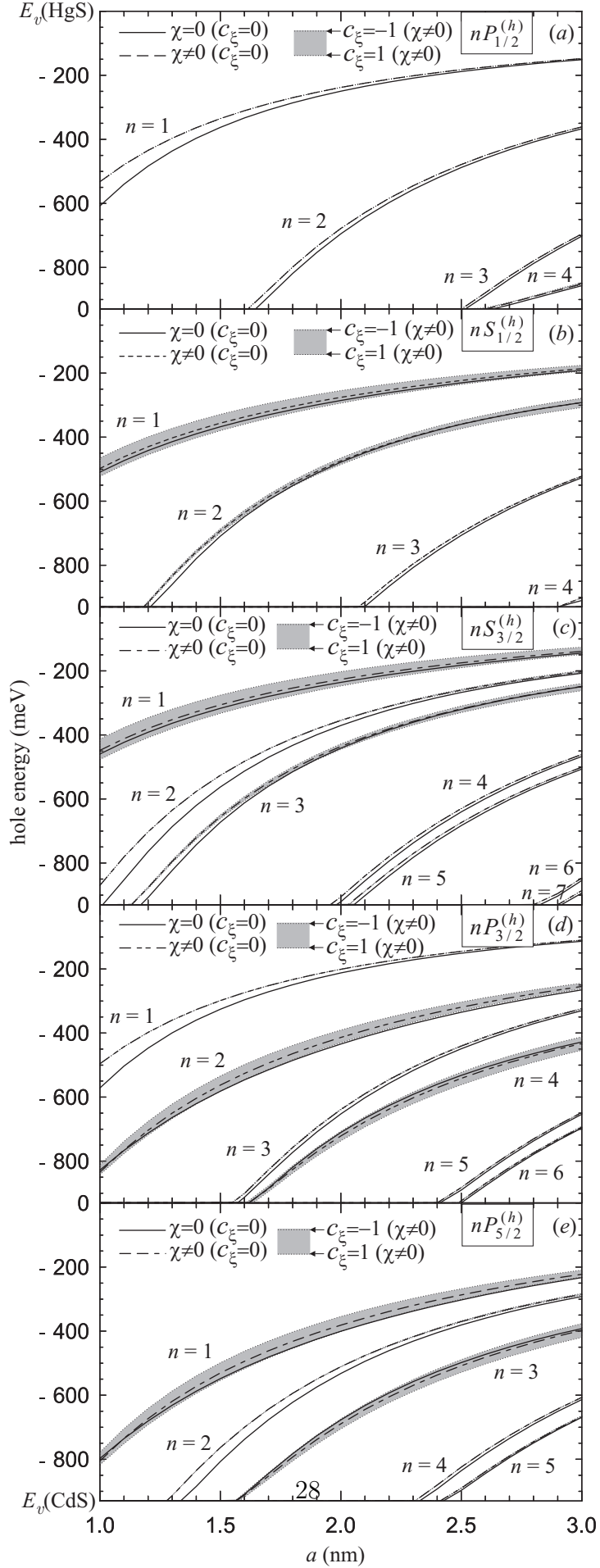


FIG. 4. All the hole energy levels of $G_{1/2}^{(h)}$ dots in the HgS/CdS QDs for different quantum dot sizes.

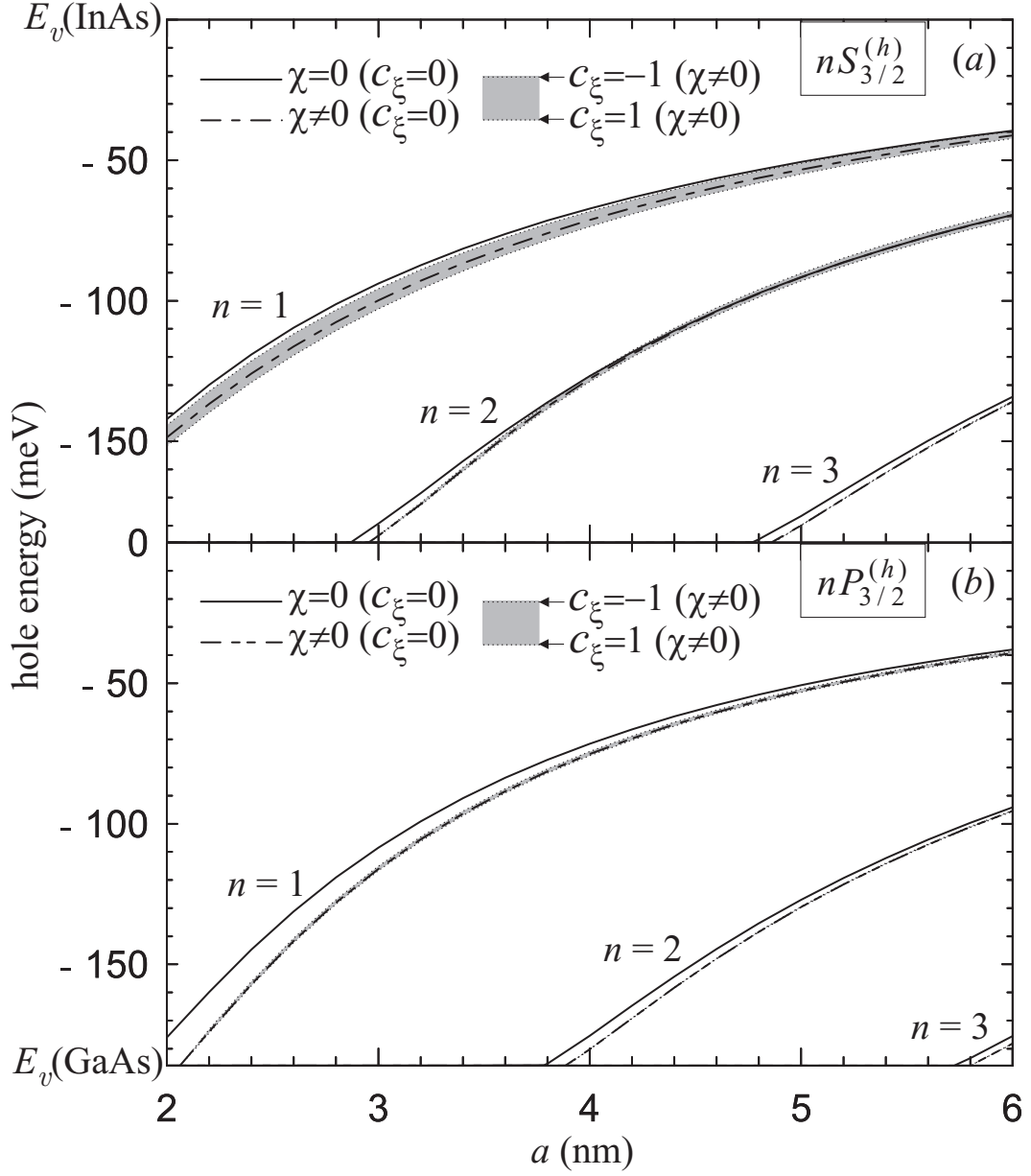


FIG. 5. All the discrete hole energy levels with $j = 3/2$ in the InAs/GaAs QDH as a function of the quantum dot radius. Other denotations are the same as in Fig. 1.

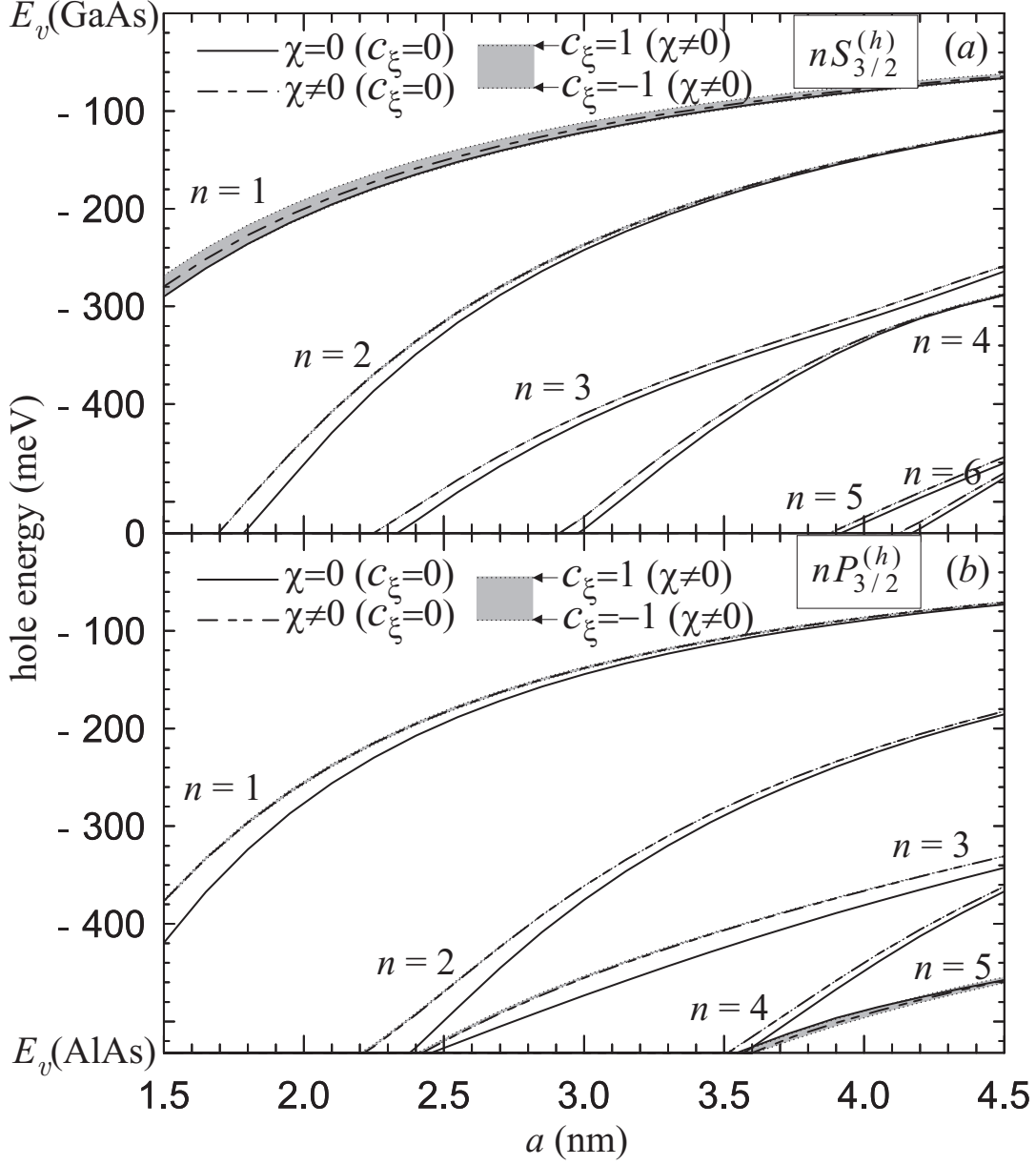


FIG. 6. All the discrete hole energy levels with $j = 3/2$ in the GaAs/AlAs QDH as a function of the quantum dot radius. Other denotations are the same as in Fig. 1.

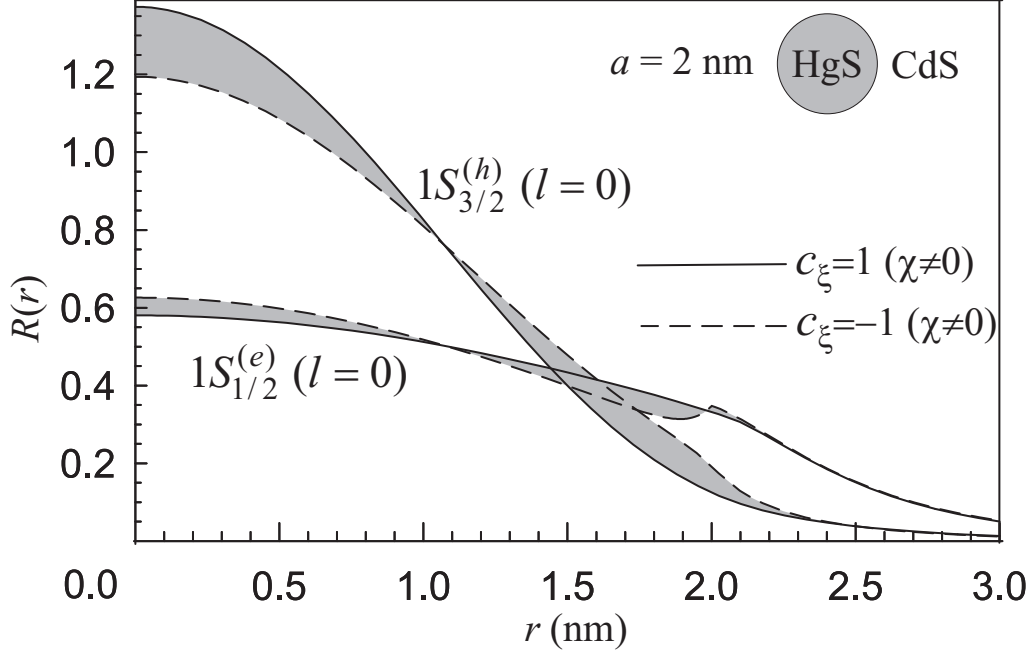


FIG. 7. S -type radial components of the wave functions of the electron and hole ground states in the HgS/CdS QDH (radius $a = 2 \text{ nm}$) within the nonsymmetrized 8-band model. Solid and dashed lines denote the cases $c_{\xi} = 1$ and $c_{\xi} = -1$, correspondingly, while gray bands represent the continuous change of c_{ξ} within these limits. Each radial wave function is normalized by unity, i.e. the integral probability $\sum_{\mu} \int_0^{\infty} r^2 R_{\mu}^2(r) dr = 1$, where μ labels the radial components. Contributions to the integral probability from the depicted radial components vary from 68.6 % to 64.8 % for an electron and from 74.3 % to 81.1 % for a hole when c_{ξ} changes from 1 to -1 . At the same time the electron energy changes from 533.6 meV to 678.8 meV and the hole energy changes from -247.2 meV to -202.1 meV .

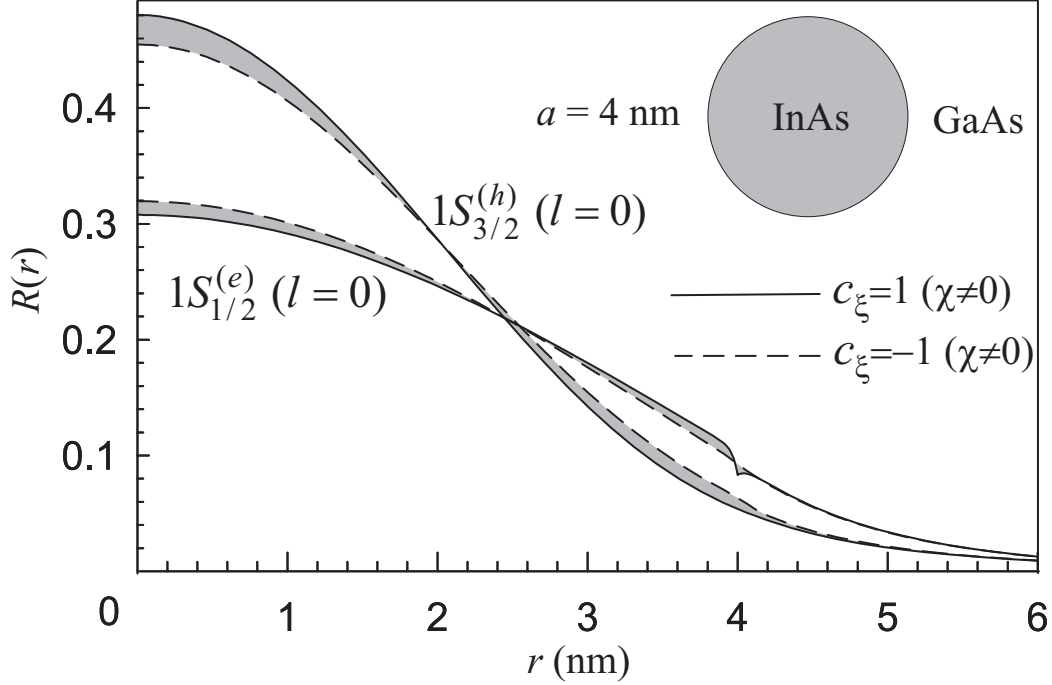


FIG. 8. S -type radial components of the wave functions of the electron and hole ground states in the InAs/GaAs QDH (radius $a = 4$ nm) within the nonsymmetrized 8-band model. Normalization of each radial wave function and denotations are same as in Fig. 7. Contributions to the integral probability from the depicted radial components vary from 80.6 % to 79.2 % for an electron and from 75.3 % to 78.7 % for a hole when c_{ξ} changes from 1 to -1 . At the same time the electron energy changes from 736.0 meV to 757.1 meV and the hole energy changes from -73.6 meV to -68.2 meV.

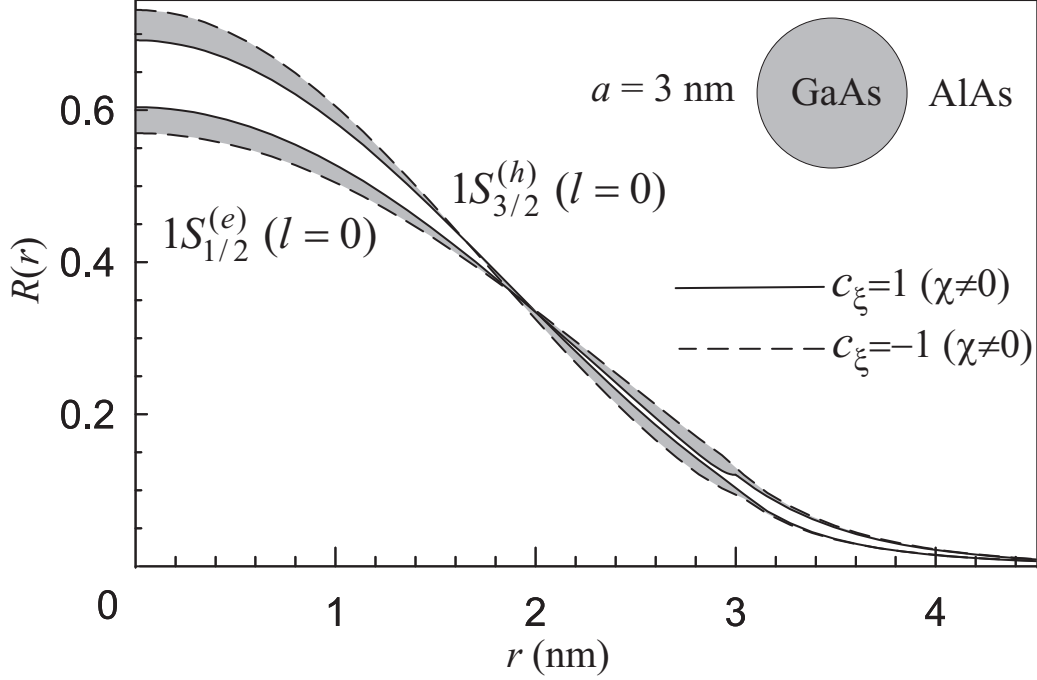


FIG. 9. S -type radial components of the wave functions of the electron and hole ground states in the GaAs/AlAs QDH (radius $a = 3$ nm) within the nonsymmetrized 8-band model. Normalization of each radial wave function and denotations are the same as in Fig. 7. Contributions to the integral probability from the depicted radial components vary from 85.4 % to 86.9 % for an electron and from 88.9 % to 86.6 % for a hole when c_{ξ} changes from 1 to -1 . At the same time the electron energy changes from 1880.4 meV to 1850.4 meV and the hole energy changes from -111.6 meV to -122.9 meV.

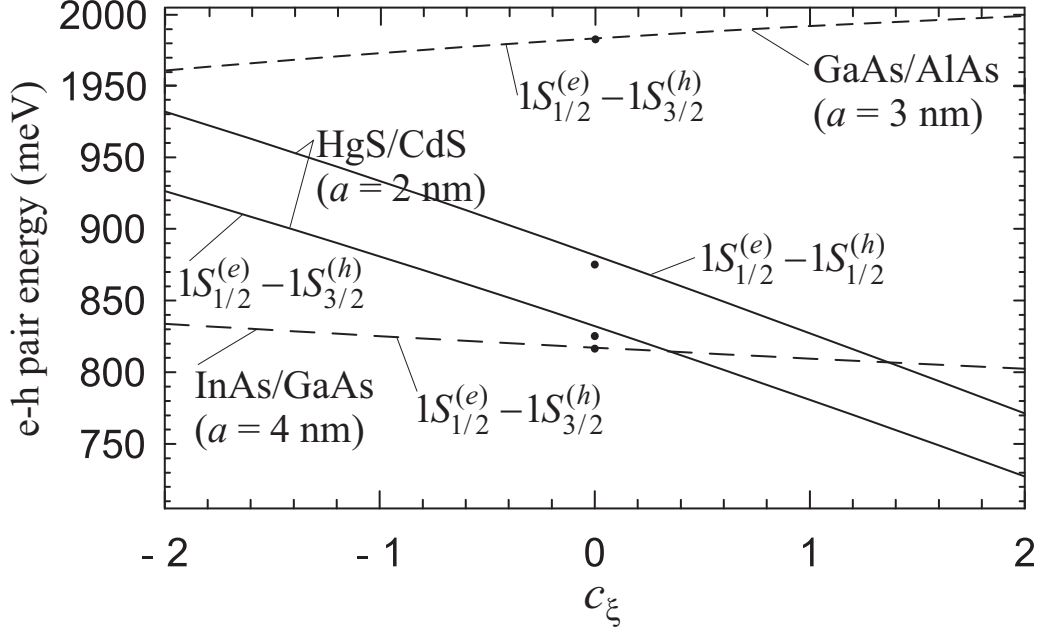


FIG. 10. The lowest electron-hole pair energies in different QDHs as a function of c_ξ ($\chi \neq 0$). Each dot is related to the closest curve and indicates the corresponding result of the symmetrized model ($c_\xi = 0$, $\chi = 0$).

REFERENCES

- [†] Electronic address: pokatilov@add.moldova.su
- [‡] Electronic address: fonobero@usm.md
- [§] Permanent address: Laboratory of Multilayer Structure Physics, Department of Theoretical Physics, State University of Moldova, A. Mateevici 60, MD-2009 Chişinău, Moldova. Electronic address: fomin@uia.ua.ac.be
- ^{*} Also at: Universiteit Antwerpen (RUCA), Groenenborgerlaan 171, B-2020 Antwerpen, België and Technische Universiteit Eindhoven, P. O. Box 513, 5600 MB Eindhoven, The Netherlands. Electronic address: devreese@uia.ua.ac.be
- ¹ J. M. Luttinger and W. Kohn, Phys. Rev. **97**, 869 (1955).
- ² A. Baldereschi and N. O. Lipari, Phys. Rev. B **8**, 2697 (1973).
- ³ J. B. Xia, Phys. Rev. B **40**, 8500 (1989).
- ⁴ V. M. Fomin, V. N. Gladilin, J. T. Devreese, E. P. Pokatilov, S. N. Balaban, and S. N. Klimin, Phys. Rev. B **57**, 2415 (1998).
- ⁵ G. B. Grigoryan, E. Kazaryan, Al. L. Efros, and T. V. Yazeva, Sov. Phys. Solid State **32**, 1031 (1990).
- ⁶ A. I. Ekimov, F. Hache, M. C. Schanne-Klein, D. Ricard, C. Flitzanis, I. A. Kudryavtzev, T. V. Yazeva, A. V. Rodina, and Al. L. Efros, J. Opt. Soc. Am. B **10**, 100 (1993).
- ⁷ C. R. Pidgeon and R. N. Brown, Phys. Rev. **146**, 575 (1966).
- ⁸ P. C. Sercel and K. J. Vahala, Phys. Rev. B **42**, 3690 (1990).
- ⁹ Al. L. Efros and M. Rosen, Phys. Rev. B **58**, 7120 (1998).
- ¹⁰ F. M. Gashimzade, A. M. Babaev, and M. A. Bagirov, J. Phys.: Condens. Matter **12**, 7923 (2000).
- ¹¹ P. C. Sercel, Al. L. Efros, and M. Rosen, Phys. Rev. Lett. **83**, 2394 (1999).
- ¹² C. Pryor, Phys. Rev. B **57**, 7190 (1998).
- ¹³ O. Stier, M. Grundmann, and D. Bimberg, Phys. Rev. B **59**, 5688 (1999).
- ¹⁴ J. M. Shi, V. N. Freire, and G. A. Farias, Eur. Phys. J. B **14**, 337 (2000).
- ¹⁵ Ch.-Y. Hsieh, D.-S. Chuu, and Ch.-Y. Hsieh, J. Phys.: Condens. Matter **12**, 8641 (2000).
- ¹⁶ W. Jaskolski and G. W. Bryant, Phys. Rev. B **57**, R4237 (1998).
- ¹⁷ E. P. Pokatilov, V. A. Fonoberov, V. M. Fomin, S. N. Klimin, and J. T. Devreese, Bullet. Amer. Phys. Soc. **45**, 988 (2000).
- ¹⁸ M. V. Kisin, B. L. Gelmont, and S. Luryi, Phys. Rev. B **58**, 4605 (1998).
- ¹⁹ M. G. Burt, J. Phys.: Condens. Matter **4**, 6651 (1992).
- ²⁰ M. G. Burt, Phys. Rev. B **50**, 7518 (1994).
- ²¹ M. G. Burt, J. Phys.: Condens. Matter **11**, R53 (1999).
- ²² B. A. Foreman, Phys. Rev. Lett. **80**, 3823 (1998).
- ²³ G. Bastard, Phys. Rev. B **24**, 5693 (1981).
- ²⁴ Y. R. Lin-Liu and L. J. Sham, Phys. Rev. B **32**, 5561 (1985).
- ²⁵ G. A. Baraff and D. Gershoni, Phys. Rev. B **43**, 4011 (1991).
- ²⁶ C. Y.-P. Chao and S. L. Chuang, Phys. Rev. B **46**, 4110 (1992).
- ²⁷ G. Edwards, E. C. Valadares, and F. W. Sheard, Phys. Rev. B **50**, 8493 (1994).
- ²⁸ B. A. Foreman, Phys. Rev. B **48**, 4964 (1993).
- ²⁹ B. A. Foreman, Phys. Rev. B **56**, R12748 (1997).
- ³⁰ R. van Dalen and P. N. Stavrinou, Semicond. Sci. Technol. **13**, 11 (1998).
- ³¹ F. Mireles and S. E. Ulloa, Phys. Rev. B **60**, 13659 (1999).

- ³² F. Mireles and S. E. Ulloa, Phys. Rev. B **62**, 2562 (2000).
- ³³ A. T. Meney, B. Gonul, and E. P. O'Reilly, Phys. Rev. B **50**, 10893 (1994).
- ³⁴ S. De Franceschi, J. M. Jancu, and F. Beltram, Phys. Rev. B **59**, 9691 (1999).
- ³⁵ L. W. Wang, Phys. Rev. B **61**, 7241 (2000).
- ³⁶ D. J. BenDaniel and C. B. Duke, Phys. Rev. **152**, 683 (1966).
- ³⁷ S. Adachi, *Physical Properties of III-V Semiconductor Compounds* (John Wiley & Sons, New York, 1992).
- ³⁸ S. L. Chuang, *Physics of Optoelectronic Devices* (John Wiley & Sons, New York, 1995).
- ³⁹ Landolt-Börnstein, *Numerical Data and Functional Relationships in Science and Technology*, New Series (Springer, Berlin, 1982), Vol. III/17a.
- ⁴⁰ *Properties of Aluminium Gallium Arsenide*, edited by S. Adachi (INSPEC, London, 1993).
- ⁴¹ K. Dybko, W. Szuszkiewicz, E. Dynowska, W. Paszkowicz, and B. Witkowska, Physica B **256**, 629 (1998).
- ⁴² $\gamma_1 + 2\gamma = -1.0$ is taken from Ref. 41 and $\gamma_1 - 2\gamma = 1.696$ is taken from Ref. 43.
- ⁴³ M. von Truchsess, A. Pfeuffer-Jeschke, C. R. Becker, G. Landwehr, and E. Batke, Phys. Rev. B **61**, 1666 (2000).
- ⁴⁴ P. Lawaetz, Phys. Rev. B **4**, 3460 (1971).
- ⁴⁵ A. H. Nethercot, Phys. Rev. Lett. **33**, 1088 (1974).
- ⁴⁶ C. Hermann and C. Weisbuch, Phys. Rev. B **15**, 823 (1977).
- ⁴⁷ Parameters m_c , γ_1^L , and γ^L are computed applying the quasicubic model⁴⁸ (i.e. $1/m_c = (2/m_{c\perp} + 1/m_{c\parallel})/3$, $\gamma_1^L = (2/m_{\perp}^A + 1/m_{\parallel}^A)/3$, $\gamma^L = (1/m_{\perp}^A - 1/m_{\parallel}^A)/3$) to the effective masses of wurtzite CdS. $m_{c\perp}$, $m_{c\parallel}$, m_{\perp}^A , m_{\parallel}^A were determined in Ref. 49, using the empirical pseudopotential method.
- ⁴⁸ Yu. M. Sirenko, J. B. Jeon, K. W. Kim, M. A. Littlejohn, and M. A. Stroscio, Phys. Rev. B **53**, 1997 (1996).
- ⁴⁹ J. B. Xia and J. Li, Phys. Rev. B **60**, 11540 (1999).